The Whale Mountain allochthon: A relic of the Iapetus Ocean preserved in the northeastern Brooks Range of Alaska and Yukon

Benjamin G. Johnson

Department of Geology and Geography, West Virginia University, Morgantown, West Virginia 26506, USA

Justin V. Strauss

Department of Earth Sciences, Dartmouth College, Hanover, New Hampshire 03755, USA

John F. Taylor

Department of Geoscience, Indiana University of Pennsylvania, Indiana, Pennsylvania 15705, USA

William P. Ward

Department of Earth and Environmental Sciences, University of Iowa, Iowa City, Iowa 52242, USA

Maurice Colpron

Yukon Geological Survey, Whitehorse, Yukon YIA 2C6, Canada

William C. McClelland

Department of Earth and Environmental Sciences, University of Iowa, Iowa City, Iowa 52242, USA

Jaime Toro

Department of Geology and Geography, West Virginia University, Morgantown, West Virginia 26506, USA

ABSTRACT

The Whale Mountain allochthon is a structural complex composed of lower Paleozoic mafic volcanic and marine sedimentary rocks that are exposed within three fault-bounded, east-west-trending belts in the northeastern Brooks Range of Alaska and Yukon. Each belt is characterized by a unique structural and stratigraphic architecture. Trace-element systematics from the volcanic rocks define distinctive suites that are geographically restricted to each belt. The volcanic rocks of the southern belt (the Marsh Fork volcanic rocks) have a tholeiitic character and rare earth element trends that resemble modern mid-ocean-ridge basalt. The volcanic rocks of the central belt (the Whale Mountain volcanic rocks) and northern belt (Ekaluakat formation; new name) both have an alkaline character, but the northern belt rocks are significantly more enriched in the incompatible trace elements. New zircon U-Pb data from two volcaniclastic rock units, one from the southern belt and another from central belt, yield unimodal age populations that range from ca. 567

Johnson, B.G., Strauss, J.V., Taylor, J.F., Ward, W.P., Colpron, M., McClelland, W.C., and Toro, J., 2018, The Whale Mountain allochthon: A relic of the Iapetus Ocean preserved in the northeastern Brooks Range of Alaska and Yukon, *in* Piepjohn, K., Strauss, J.V., Reinhardt, L., and McClelland, W.C., eds., Circum-Arctic Structural Events: Tectonic Evolution of the Arctic Margins and Trans-Arctic Links with Adjacent Orogens: Geological Society of America Special Paper 541, https://doi.org/10.1130/2018.2541(20). © 2018 The Geological Society of America. All rights reserved. For permission to copy, contact editing@geosociety.org.

to 474 Ma, with weighted averages of 504 ± 11 and 512 ± 1.4 Ma for each sample. In the central and southern belts of the allochthon, basalt flows are interbedded with discontinuous limestone and dolostone units that contain trilobites and agnostoid arthropods. Three distinct trilobite faunas of late Cambrian (Furongian) age were recovered from widely separated localities. The scarcity of uniquely Laurentian genera, coupled with an abundance of distinctive species that could not be assigned to any established Furongian genus, argues against models that invoke extrusion of these volcanic rocks onto the autochthonous Laurentian shelf or slope. It is thus proposed that the Whale Mountain allochthon formed in a peri-Laurentian setting, possibly as disparate fragments of the northern Iapetus Ocean that were assembled in an ancient accretionary wedge and subsequently accreted to the northern margin of Laurentia during the early Paleozoic.

INTRODUCTION

Dense oceanic lithosphere is consumed by subduction at convergent margins, erasing most, if not all, evidence of the ancient seafloor from the geologic record. In rare cases, however, relics of ancient ocean basins are preserved within orogenic belts in the form of ophiolites or fragments of oceanic crust, scraped off a subducting plate and entrained into an accretionary wedge. The Iapetus Ocean, the early Paleozoic ancestor to the modern Atlantic Ocean, is a classic example of an ancient ocean basin where the geologic record has largely been destroyed by subduction and the suturing of several large paleocontinents (e.g., van Staal et al., 1998). Disconnected tracts of ophiolites and oceanic fragments scattered along the Northern Appalachians (van Staal and Barr, 2012), the British Isles (Chew and Strachan, 2014), and the Scandinavian Caledonides (Corfu et al., 2014) mark the sparse remains of the Iapetus Ocean.

Paleogeographic reconstructions have postulated a continuation of the Iapetus suture into the paleo-Arctic realm (e.g., Lawver, et al., 2002; Colpron and Nelson, 2011; Miller et al., 2011; Pease, 2011; Beranek et al., 2013; Strauss et al., 2017; Hoiland et al., 2017). The composite Arctic Alaska terrane, sometimes grouped within the larger Arctic Alaska-Chukotka microplate (e.g., Miller et al., 2006), is prominently featured in the paleogeographic reconstructions of the Arctic. An abundance of recent geochronological and paleontological evidence suggests that the various subterranes that compose the greater Arctic Alaska terrane can be assigned to at least three separate paleogeographic affinities at the time of Iapetus closure. Southern Arctic Alaska includes the Seward, Hammond, Slate Creek, and Coldfoot subterranes of Moore et al. (1994). Recently, Hoiland et al. (2017) grouped these into a single southern Brooks Range terrane because they share early Paleozoic affinities with northern Baltica (e.g., Patrick and McClelland, 1995; Dumoulin et al., 2002; Amato et al., 2009, 2014; Miller et al., 2011). The northern half of the Arctic Alaska terrane is contained within the North Slope subterrane (herein simplified to the North Slope), which is unequivocally linked to Laurentia (Strauss et al., 2013; McClelland et al., 2015; Lane et al., 2016; Johnson et al., 2016).

Residing along the boundary zone between the southern Brooks Range terrane and the North Slope is the Cambrian(?)–Silurian Doonerak arc complex, which was recently inferred by Strauss et al. (2017) to have formed contemporaneously with Taconic–Caledonian arc magmatism along the northeastern edge of Laurentia, thereby preserving a relic of the Iapetus suture within the Arctic Alaska terrane.

An enduring issue involving the paleogeographic restorations of Arctic Alaska relates to the early Paleozoic position of the North Slope along the northern margin of Laurentia. Some researchers have argued that the North Slope restores to northeastern (NE) Laurentia, citing similarities between the rocks exposed in the NE Brooks Range (Fig. 1), which belongs to the North Slope, and Ellesmere Island in Arctic Canada (Sweeney, 1982; Strauss et al., 2013; Cox et al., 2015; Johnson et al., 2016). Others have argued that the North Slope remained fixed to northwestern (NW) Laurentia, calling for stratigraphic continuity between strata exposed in the NE Brooks Range and the Selwyn Basin of central Yukon and elsewhere in the Canadian Cordillera (Cecile et al., 1999; Lane, 2007; Lane et al., 2016).

A principal component in these debates relates to the tectonic and depositional setting of the upper Cambrian Whale Mountain volcanic rocks, exposed in the NE Brooks Range. Based on the alkaline geochemistry of the volcanic rocks and putative similarities with mafic volcanic rocks in northern Canada, Lane et al. (2016) argued that these volcanic rocks erupted within the continental margin of northwestern (NW) Laurentia. Conversely, Johnson et al. (2016) argued that the volcanic rocks in the NE Brooks Range were fault-bounded and instead belonged to an exotic Cambrian-Ordovician oceanic fragment, which they named the Whale Mountain allochthon. The interpretations of Lane et al. (2016) and Johnson et al. (2016), however, both fundamentally relied on sparse geochemical data from previous reconnaissance studies (Moore, 1987; Goodfellow et al., 1995), and the biostratigraphic data available to constrain the age and paleogeographic affinities of the Whale Mountain allochthon were limited and imprecise. The limited faunal control was particularly problematic, in that the endemic faunas that evolved on the Laurentian platform during the Cambrian provide the most definitive means of discriminating strata that originated on or adjacent to that paleocontinent from exotic packages that arrived subsequently through accretion. Here, we provide new field observations coupled with additional geochronological, geochemical, and paleontological data from the Whale Mountain volcanic rocks and other associated units in the NE Brooks Range that support a peri-Laurentian oceanic origin for the Whale Mountain allochthon.

GEOLOGICAL SETTING

The high topography of the NE Brooks Range forms a structural salient that protrudes more than 100 km northward from the main front of the Brook Range and stretches from the Canning River in Alaska into northern Yukon (Fig. 1). It is a critical region for geological investigation because it exposes a prominent angu-

lar unconformity (Figs. 1 and 2) that separates Lower Mississippian quartz-rich siliciclastic units of the Endicott Group (Brosgé et al., 1962) from a thick (>2000 m) succession of tightly folded and weakly metamorphosed, Neoproterozoic to lower Paleozoic sedimentary and igneous rocks (pre-Mississippian sequence of Moore et al., 1994).

The sub-Mississippian rocks in the NE Brooks Range have been investigated using a variety of different map and stratigraphic schemes (see Strauss et al., this volume, Chapter 23, and references therein for a review). Initially, the Whale Mountain volcanic rocks were assigned to the "volcanic and carbonate member" of the broadly defined Neruokpuk Formation of Dutro et al. (1972). These workers split the Neruokpuk Formation into six regional sequences, lettered A through F, with the "volcanic and carbonate member" concentrated in parts of sequences A and C. Critically, Dutro et al. (1972) also recovered trilobite

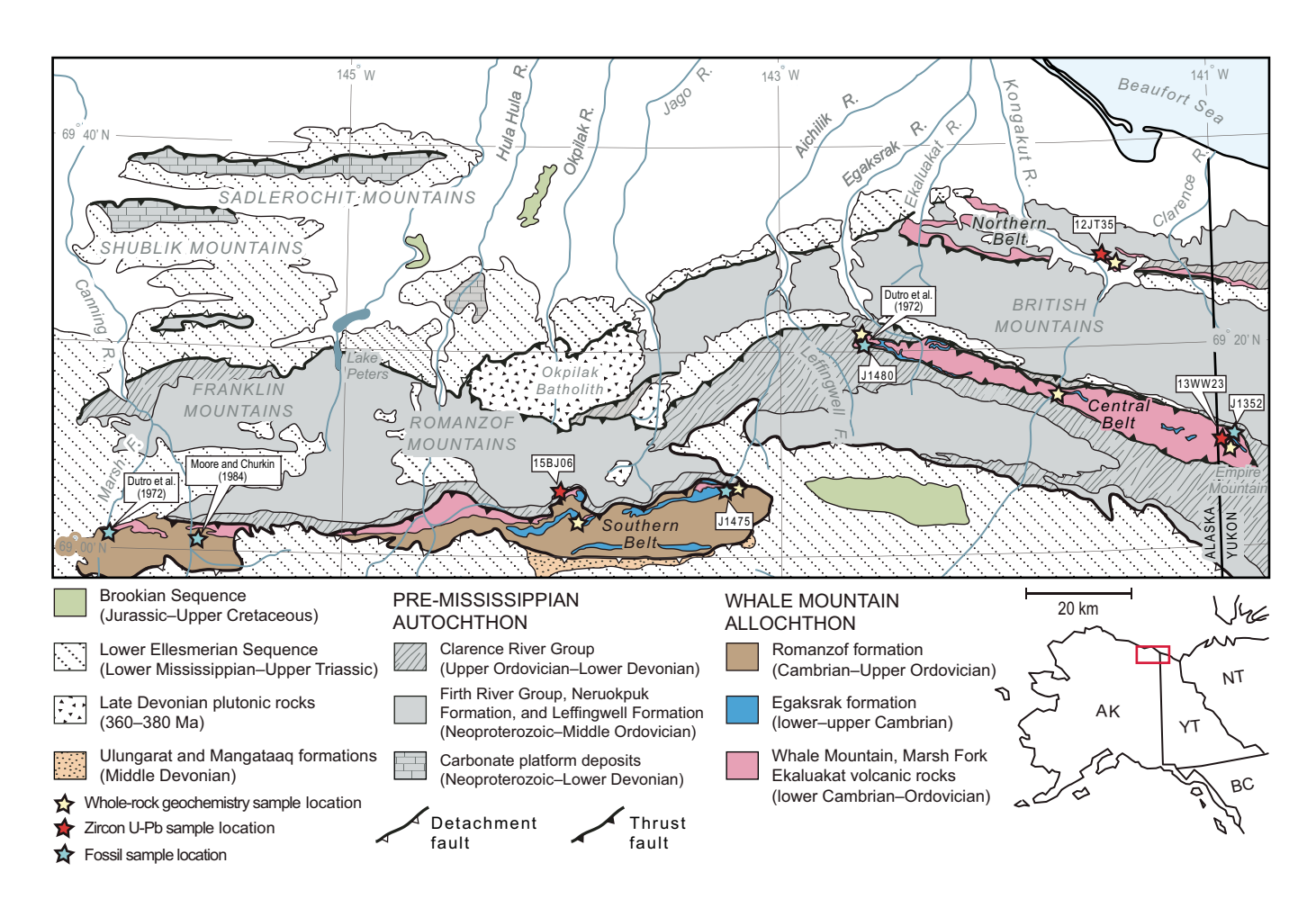


Figure 1. Simplified geologic map of the eastern half of the NE Brooks Range, Alaska, highlighting the distribution of rocks comprising the Whale Mountain allochthon and sample locations. The map is modified from Reiser et al. (1980), Wallace and Hanks (1990), Mull and Anderson (1991), Lane et al. (1995), and Johnson et al. (2016). Solid teeth on thrust faults indicate disruption of stratigraphic section (old-on-young); open teeth indicate detachment surfaces along which there has been slip but no disruption of the stratigraphic section (young-on-old). Sample numbers are described in the text and outlined in file DR1 of the GSA Data Repository (see text footnote 1). Sample 12JT35 in the northern belt is from Johnson et al. (2016), and sample 14BJ25 is from Strauss et al. (this volume, Chapter 23). Inset abbreviations: AK—Alaska; YT—Yukon; NT—Northwest Territories; BC—British Columbia.

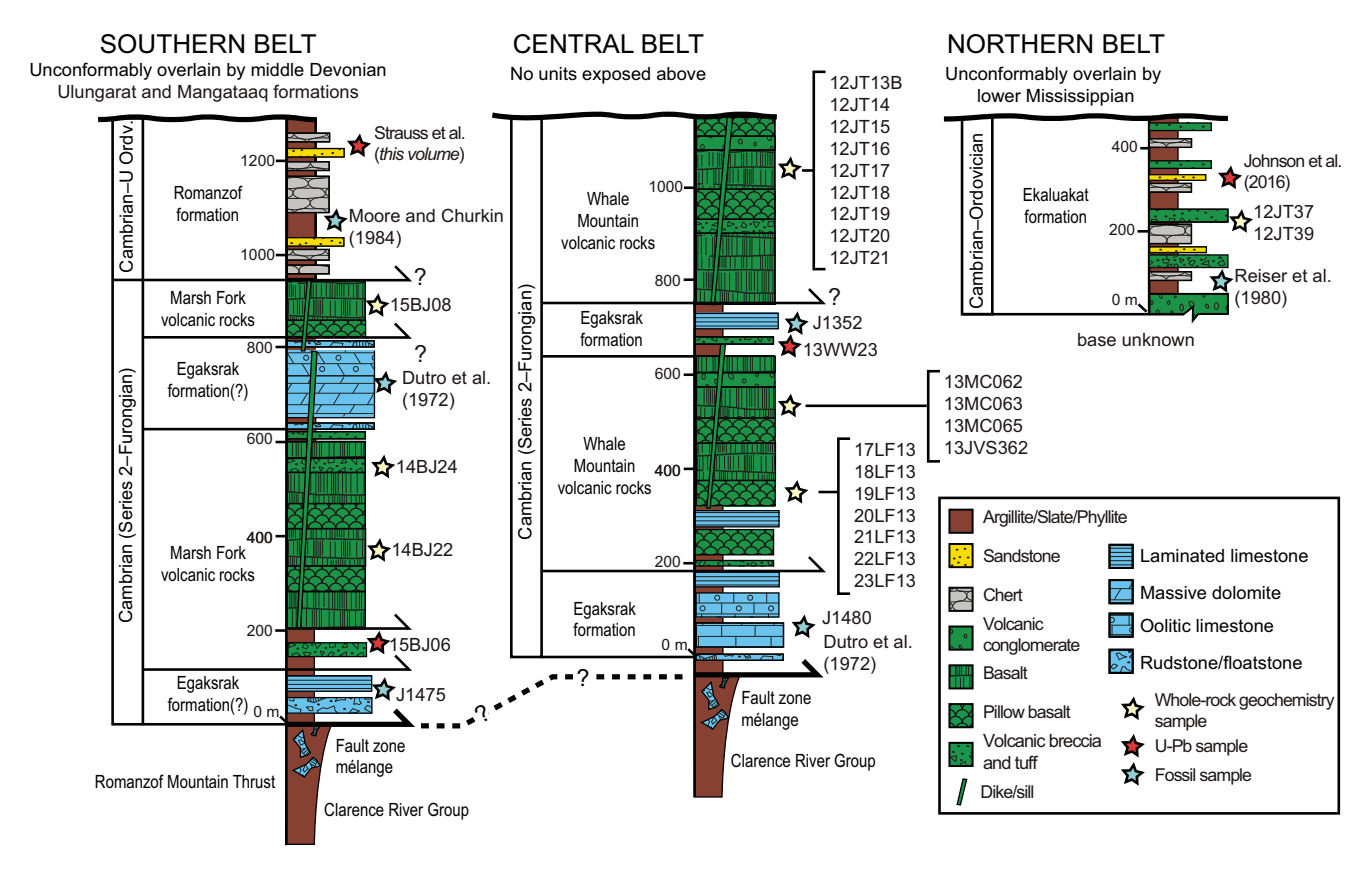


Figure 2. Schematic lithostratigraphy of the southern, central, and northern belts of the Whale Mountain allochthon. Thicknesses are approximated from generalized field observations. U Ordv.—Upper Ordovician.

and brachiopod fossils from the "volcanic and carbonate member" at two localities, one along the Marsh Fork of the Canning River, and another along the Leffingwell Fork of the Aichilik River (Fig. 1). The Marsh Fork locality yielded olenellid trilobites of early Cambrian age, whereas the Leffingwell Fork locality yielded trilobites and brachiopods of late Cambrian age (middle Furongian).

Although Dutro et al. (1972) treated the Neruokpuk Formation as a somewhat coherent stratigraphic package, they, along with an earlier study by Reiser (1970), recognized that a regional thrust fault disrupted parts of the stratigraphic order. The fault was mapped along the base of the volcanic rocks of sequence A in the headwaters of the Aichilik, Jago, Hulahula, and Canning rivers in the Romanzof Mountains, and it was inferred to be concealed by the sub-Mississippian unconformity. Later, during the compilation of the 1:250,000 scale Demarcation Point geologic quadrangle by Reiser et al. (1980), the sequence nomenclature was abandoned, and the Neruokpuk name was reverted to the original usage of Leffingwell (1919), which restricts the Neruokpuk to the "quartzite and semischist member" of Dutro et al. (1972). The volcanic and carbonate member was also split into two map units: a "Cambrian volcanic and volcaniclastic" unit (Cv) and a "Cambrian limestone" unit (Cl).

Some of the thickest exposures of the volcanic and carbonate rocks occur at Whale Mountain in Alaska, where an ~100-kmlong, E-W-trending synclinal exposure cuts perpendicularly across the middle reaches of the Kongakut River (Fig. 1). Moore (1987) informally named the volcanic rocks exposed along the ridge the Whale Mountain volcanic rocks, which also included the volcanic rocks exposed at the Leffingwell Fork fossil locality of Dutro et al. (1972), where Moore (1987) analyzed three samples for whole-rock geochemistry. These data, along with a second suite of volcanic samples collected by Goodfellow et al. (1995) from the Yukon segment of the Whale Mountain ridge system, showed that the Whale Mountain volcanic rocks are enriched in incompatible elements (e.g., Ti, Zr, Nb) and resemble alkaline basalt. Moore (1987) also analyzed eight volcanic samples from exposures along strike at the Marsh Fork locality of Dutro et al. (1972), which were independently assigned to the Marsh Fork volcanic rocks. Moore (1987) showed that the Marsh Fork volcanic rocks had comparable levels of incompatible element enrichment as the alkaline Whale Mountain volcanic rocks to the north; however, a few samples had more transitional and tholeiitic compositions.

A separate unit of volcanic rocks was delineated in the northern British Mountains on the map of Reiser et al. (1980).

These volcanic rocks extend from the Ekaluakat River in Alaska to the Clarence River at the Alaska–Yukon border (Fig. 1). They were originally included in sequence E of Dutro et al. (1972) but were later reassigned to the "Ordovician volcaniclastic and volcanic rocks" (Ovc) map unit by Reiser et al. (1980). The Ordovician age was constrained by a graptolite locality in an adjacent "Ordovician black slate" (Os) map unit, which was tentatively mapped beneath the volcanic rocks. From mapping studies along the Alaska–Yukon border, the volcanic rocks exposed in the Clarence River region were correlated to the thick volcanic flows at Whale Mountain to the south on the basis of lithologic similarity and an apparent gradational contact with *Oldhamia*-bearing argillite beds (Lane, 1991; Kelley et al., 1994; Lane et al., 1995).

Two recent studies, one by Lane et al. (2016) and another by Johnson et al. (2016), have placed these previously described volcanic rocks of the NE Brooks Range into different stratigraphic positions. In the scheme of Lane et al. (2016), the volcanic rocks, which they named the informal "Whale Mountain formation," reside within a semiconformable succession of Neoproterozoic-Devonian strata. This agrees with previous interpretations from field work conducted in the Clarence River region and along the Alaska-Yukon border (Lane, 1991; Kelley et al., 1994; Lane et al., 1995). Lane et al. (2016) further argued that the volcanic rocks along the Alaska-Yukon border correlate to the Marsh Fork volcanic rocks of Moore (1987), and that these volcanic rocks are all paleogeographic equivalents of volcanic rocks exposed within the Selwyn Basin of central Yukon and elsewhere in the northern Canadian Cordillera (e.g., Goodfellow et al., 1995). Critically, this correlation fixes the North Slope to NW Laurentia in the early Paleozoic, suggesting that the Whale Mountain volcanic rocks formed in response to periods of extension along the paleo-Pacific margin.

The scheme of Johnson et al. (2016) is different in that it places the volcanic rocks of the NE Brooks Range within a fault-bounded oceanic assemblage called the Whale Mountain allochthon. Based on mapping along the Kongakut River and Leffingwell Fork in Alaska, coupled with detrital zircon U-Pb and muscovite ⁴⁰Ar/³⁹Ar geochronology, Johnson et al. (2016) showed that the upper Cambrian Whale Mountain volcanic rocks of Moore (1987) overlie a Upper Ordovician-Lower Devonian(?) succession of interbedded shale, argillite, and lithic-rich sandstone. These sedimentary units were correlated to a similar succession of strata mapped in the Clarence River region along the Alaska-Yukon border (Lane, 1991; Kelley et al., 1994; Lane et al., 1995), which enabled Johnson et al. (2016) to apply the informal Clarence River group name (formalized to the Clarence River Group by Strauss et al., this volume, Chapter 23) to include all similar strata in the NE Brooks Range. This also included the siltstone, shale, sandstone, and lithic-rich pebble conglomerate units exposed in the Buckland Hills of northern Yukon, which Lane et al. (2016) originally assigned to the Lower Devonian "Buckland Hills succession" (updated to the Buckland Hills formation by Strauss et al., this volume, Chapter 23). Johnson et al. (2016) contended that detrital zircon signatures from the Clarence River Group closely resembled those of sedimentary units in the deep-water Franklinian Basin of Ellesmere Island, Arctic Canada (e.g., Beranek et al., 2015). In addition, Johnson et al. (2016) postulated that the emplacement of the Whale Mountain allochthon occurred in concert with protracted terrane accretion in NE Laurentia and the presumed closure of the northern Iapetus Ocean during the Caledonian orogeny.

STRUCTURAL AND STRATIGRAPHIC ARCHITECTURE

Here, we provide updated lithological descriptions and field observations from the volcanic and sedimentary rocks of the Whale Mountain allochthon in the NE Brooks Range of Alaska and Yukon that were assembled during a series of field campaigns conducted over the course of 5 years (2011–2015). In addition, we put forth new informal terminology for previously unnamed map units (Egaksrak, Romanzof, and Ekaluakat formations), which are outlined in Figure 2. These rocks are exposed within three E–W-trending thrust sheets or belts, which we refer to as the southern, central, and northern belts (Figs. 1 and 2). These belts are separated by ~25 km, and each is defined by its own unique structural and stratigraphic architecture.

Southern Belt

The southern belt of the allochthon stretches across 100 km of the Romanzof Mountains, from the headwaters of the Aichilik River to the Marsh Fork of the Canning River (Fig. 1). Its stratigraphy consists of intensely imbricated assemblages of chert, phyllite, carbonate, and mafic volcanic and volcaniclastic rocks, which were all originally assigned to sequence A of Dutro et al. (1972). In the summer of 2014 and 2015, we conducted several traverses in the headwaters of the Aichilik and Jago Rivers, where we collected several samples for thin-section analysis, three samples for whole-rock igneous geochemical analysis (14BJ24, 14BJ22, and 15BJ08), and one volcaniclastic sample for zircon U-Pb geochronology (15BJ06). We also discovered one new fossil locality (J1475) along the Aichilik River (Figs. 1 and 3A).

The base of the southern belt section is marked by a south-dipping thrust fault (Fig. 3A), the Romanzof Mountain thrust of Johnson et al. (2016), which runs along the entire northern edge of the southern belt (Figs. 1 and 3A). Early mappers in the region (e.g., Dutro et al., 1972; Reiser et al., 1980) recognized that the fault was truncated by the sub-Mississippian unconformity at the headwaters of the Aichilik River. During our traverses of the area in 2014 and 2015, we observed that in discrete locations, the Mississippian Kekiktuk Conglomerate (lower Endicott Group) is exposed in the footwall beneath the fault, indicating that some amount of post-Mississippian displacement has occurred along this structure. In other places, the volcanic and sedimentary rocks of the Whale Mountain allochthon are in direct contact with the Upper Ordovician–Lower Devonian(?) Clarence River Group (Fig. 3A).

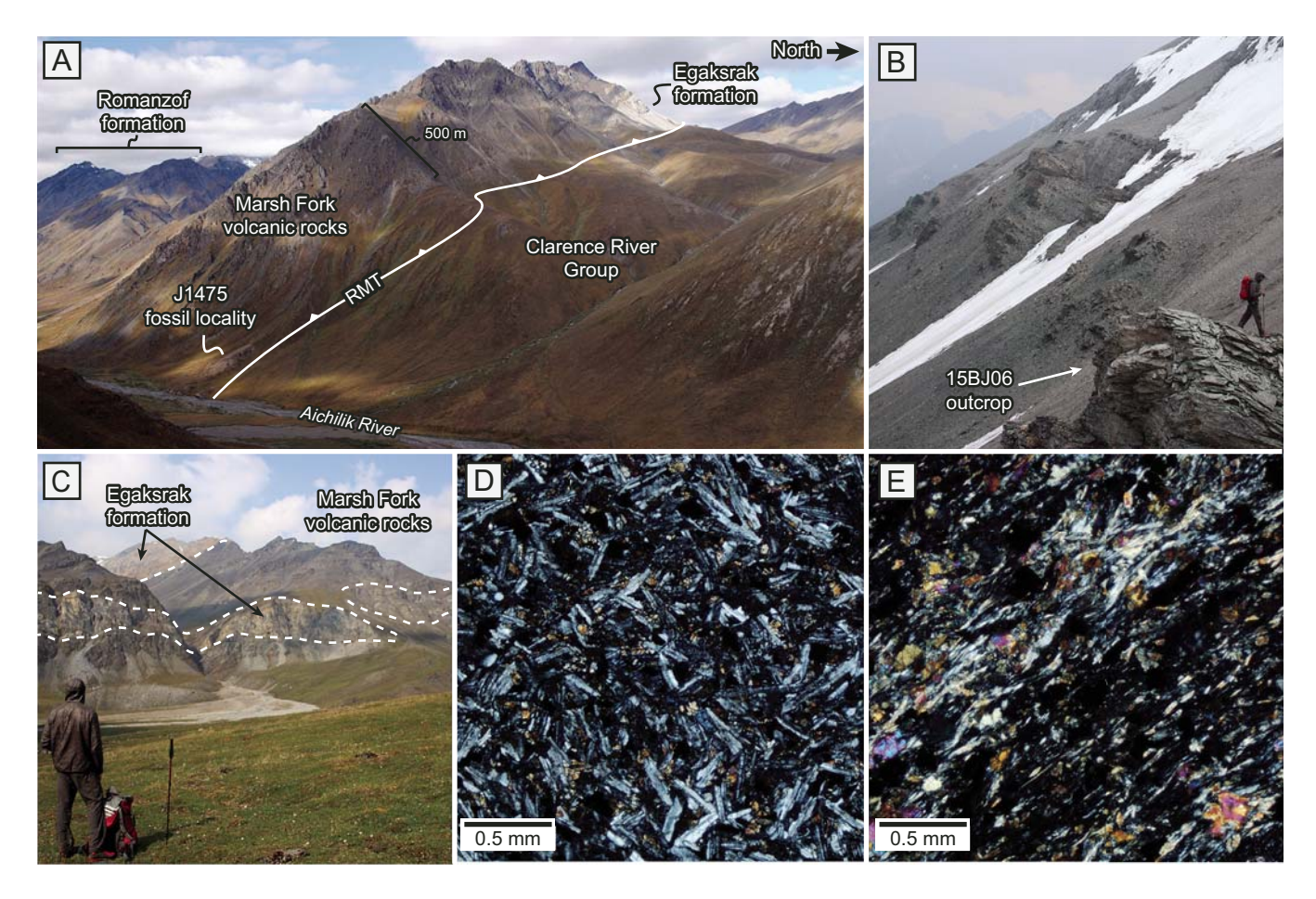


Figure 3. Field images and photomicrographs of rocks in the southern belt of the Whale Mountain allochthon in the NE Brooks Range, Alaska. (A) Looking southwest across the Romanzof Mountain thrust (RMT) at the headwaters of the Aichilik River, showing the J1475 fossil location. (B) Looking east near the fault zone of the Romanzof Mountain thrust at the headwaters of the Jago River, showing the outcrop of zircon U-Pb sample 15BJ06. (C) Looking southwest across intercalated Marsh Fork volcanic rocks and megablocks of the Egaksrak formation in the headwaters of the Jago River. (D) Cross-polarized view of sample 14BJ22 showing intergranular plagioclase phenocrysts with microcrystalline clinopyroxene. (E) Cross-polarized view of sample 15BJ08 showing aligned actinolite, epidote, plagioclase, and Fe- and Ti-oxide minerals.

The fault zone is >500 m wide in some places, and it contains a chaotic mix or mélange of different lithostratigraphic units. Along the Aichilik River, the mélange includes darkmaroon, gray, and green volcaniclastic argillite and phyllite that intertongue with discrete blocks of gray to tan-weathering dolostone and limestone. The carbonate blocks are heavily fractured and brecciated and range between ~10 and 200 m thick. Our new trilobite locality (J14745) was collected from an ~40-m-tall by 100-m-wide block within the fault zone along the western bank of the upper Aichilik River, just south of the Romanzof Mountain thrust (Fig. 3A). The rocks at the locality consist predominantly of recrystallized and locally dolomitized lime mudstone and wackestone with a pronounced volcaniclastic matrix. The fossils were recovered from an ~7-cm-thick bed of lime wackestone. Lithologically, these carbonate rocks resemble those from which Olenellus was recovered at the Marsh Fork locality of Dutro et al. (1972), but the fauna confirms a significantly younger age (see

Paleontology section below), and the structural complexity of the J1475 locality obscures further stratigraphic comparisons.

Along strike of the Romanzof Mountain thrust, in the headwaters of the Jago River, the fault zone contains a similar succession of dark-maroon, gray, and green volcaniclastic argillite and phyllite, but it is intertongued or imbricated with an ~3-m-thick massive volcaniclastic sandstone unit (Fig. 3B), which we sampled for zircon U-Pb geochronology (15BJ06). The sample consists of sheared and angular volcanic detritus (mostly plagioclase) and volcanic rock fragments. The stratigraphic assignment of this unit is uncertain, but the predominance of angular volcanic material implies a close association to the volcanic flows exposed higher in the southern belt section.

Above the fault zone, the section transitions into an ~300–800-m-thick exposure of dark-greenish gray mafic amygdaloidal volcanic flows and subordinate beds of conglomerate, volcaniclastic argillite, and chert. The mafic flows typically

show pillow structures or are brecciated, and they resemble the volcanic rocks described by Moore (1987) from the Marsh Fork area at the western limit of the southern belt. We therefore apply the Marsh Fork volcanic rocks name to these exposures. In many places, the volcanic rocks intertongue with large blocks of limestone and dolostone that sometimes exceed 200 m in thickness and cover areas as wide 10 km in length (Fig. 3C). These carbonate blocks consist of gray- and tan-weathering, massive, thickbedded oolitic and peloidal dolostone, as well as calcareous rudstone composed of angular carbonate and volcanic lithoclasts and lime mudstone horizons. Like the carbonate blocks near the fault zone, the megablocks have sharp contacts with the surrounding deformed volcanic units, which may be a product of imbrication by unmapped thrust faults or stratigraphic complexity derived through sediment-gravity flows. We tentatively assign the name Egaksrak formation to all the carbonate units in the southern belt because of lithological similarities to carbonate units in the type area between the Leffingwell Fork and the Egaksrak River (see Central Belt subsection below).

Two volcanic samples (14BJ22 and 14BJ24) were collected from the volcanic and carbonate section exposed along the Aichilik River. The samples are fine grained, sparsely porphyritic (1%–5% phenocrysts), and dominated by plagioclase (>50 vol%). Plagioclase occurs as euhedral laths, both in the groundmass (<0.5 mm in length) and as phenocrysts (>1 mm in length). The plagioclase laths in sample 14BJ22 exhibit an intergranular texture with subhedral clinopyroxene and Fe- and Ti-oxide minerals (Fig. 3D). The uniform nature of the plagioclase and the intergranular texture in these samples suggest a cumulate origin in a thick lava flow or hypabyssal intrusion. Both samples are sparsely to moderately amygdaloidal (2–10 vol%). The amygdules typically have an elongate shape, range from 0.25 to 5 mm in diameter, and are filled with chlorite group minerals or calcite. A third volcanic sample (sample 15BJ08) was collected from a 3-m-thick outcrop of greenish-gray metabasalt in the headwaters of the Jago River. These units are heavily sheared and are crosscut by an extensive network of 1-3-cm-thick serpentinite veins. The dominant mineral phases include actinolite, chlorite, epidote, and opaque minerals. Actinolite occurs as elongate subhedral prismatic crystals, up to 1 mm in length, that define a moderate foliation (Fig. 3E). Epidote occurs as rounded, subhedral grains aligned along the actinolite grain boundaries, spatially associated with opaque minerals. The metamorphic mineral assemblage of actinolite, epidote, and chlorite indicates that these rocks were subject to greenschist metamorphic conditions.

Above the volcanic and carbonate units, there is an isoclinally folded package of undetermined thickness containing interbedded radiolarian chert and phyllite with minor beds of volcanic and lithic wacke. These rocks were originally designated as the "chert and phyllite member" by Dutro et al. (1972) and were later split into the "Ordovician–Cabrian chert and phyllite" (OCcp) and the "Ordovician volcanic wacke and tuffaceous sandstone" (OCw) map units of Reiser et al. (1980). Mull and Anderson (1991) referred to this package as the Romanzof chert,

but we instead refer to this unit as the Romanzof formation due to its diversity of lithofacies. Moore and Churkin (1984) collected Middle Ordovician graptolites from a phyllite and radiolarian chert interval within the Romanzof formation near the Marsh Fork of the Canning River.

The subordinate volcanic and lithic wacke units consist of centimeter- to meter-thick beds that occasionally exhibit erosional bases with channel-fill geometries in the surrounding chert and phyllite. The wacke is generally poorly sorted and composed of fine- to medium-grained, angular to subrounded, monocrystal-line and polycrystalline quartz, plagioclase, opaque minerals, and chert and basalt lithic fragments. One detrital zircon sample was collected from these units by Strauss et al. (this volume, Chapter 23). The sample yielded 23 concordant U-Pb ages that define a unimodal population from ca. 494 to 436 Ma, with a peak at 452 Ma, suggesting that parts of the Romanzof formation are as young as Late Ordovician.

The Romanzof formation is overlain by sandstone, shale, and limestone of the Middle Devonian Ulungarat and Mangaqtaaq formations of Anderson et al. (1994). The contact relationships between these two units, however, are not well documented. Anderson et al. (1994) mapped the contact as a faulted unconformity (Aichilik Pass thrust). Because this contact is unconstrained, and because the region is structurally complex, the total estimated thickness of the southern belt section presented in Figure 2 should be treated as a structural thickness.

Central Belt

The central belt of the allochthon stretches from Empire Mountain in northern Yukon to the Leffingwell Fork of the Aichilik River in Alaska (Fig. 1). During the summers of 2012, 2013, and 2014, we traversed across three separate locations in the central belt, collecting >20 volcanic samples for thin section and geochemical analysis and one volcanic wacke sample (13WW23) for zircon U-Pb geochronology. We also discovered one new fossil locality in Yukon (J1352) and resampled the fossils from the original locality of Dutro et al. (1972) between the Leffingwell Fork and Egaksrak River (Fig. 1).

The stratigraphy of the central belt consists predominantly of intercalated volcanic and carbonate rocks (Fig. 2), which were originally assigned to the upper parts the Neruokpuk sequence C of Dutro et al. (1972). The volcanic rocks have since been assigned to the Whale Mountain volcanic rocks by Moore (1987), and we assign the carbonate units to the Egaksrak formation, due to their prominent exposure along the ridge that separates the Leffingwell Fork and the Egaksrak River. The entire central belt appears to be folded into an ~10-km-wide by ~100-km-long synclinal ridge that is >1000 m thick where it crosses the Kongakut River in Alaska and that thins to <600 m thick along the Leffingwell Fork. Like the southern belt section, the base of the central belt section is marked by a complex fault zone mélange of Clarence River Group strata mixed with large slivers of the carbonate units that range from 5 to 200 m thick.

This fault zone also appears to be broadly folded into a synform (Fig. 4A). The top of the central belt is not covered by any younger lithostratigraphic units, rendering its original stratigraphic thickness indeterminable.

At the western edge of the central belt, near the Leffingwell Fork fossil locality of Dutro et al. (1972), the fault zone becomes subhorizontal and is exposed along a broad saddle in the ridge that divides the Leffingwell Fork and the Egaksrak River (Fig. 4B). An ~200-m-thick, vertically dipping megablock of intensely sheared limestone is exposed between the black slate of the Clarence River Group and the Whale Mountain volcanic rocks higher in the section (Fig. 4B). The block includes contorted beds of discontinuous rudstone that contain angular to well-rounded, pebble- to sand-sized volcanic lithoclasts (Fig. 4C). This chaotic interval is bound to the north by a massive gray oolitic and peloidal grainstone unit that is interbedded with finely laminated fossiliferous lime mudstone and wackestone. Our fossil locality J1480 was recovered from the laminated mudstone interval, which is likely the same location from which Dutro et al. (1972) collected their sample 6983-CO. Like the carbonate units in the southern belt, the stratigraphic context of these large carbonate blocks is unclear, but the contacts with the surrounding units are typically abrupt or marked by brecciated limestone and volcanic units, suggesting a structural or an olistostromal relationship.

In other locations along the central belt, the lime mudstone units of the Egaksrak formation occur as laterally extensive, ~150-m-thick beds that crop out for >10 km and are interbedded with the volcanic rocks (Fig. 4A). Near the headwaters of the Malcolm River in Yukon, the J1352 fossil locality was discovered in fossiliferous lime and volcaniclastic mudstone, grainstone, and rudstone interbedded with pillowed Whale Mountain volcanic rocks (Fig. 4D). The fossiliferous strata include an ~15-m-thick lens of ribbon-bedded lime mudstone (Fig. 4E), fossiliferous wackestone, reworked meter-scale carbonate olistoliths and rudstone, and volcaniclastic conglomerate and sandstone within a dominantly maroon volcaniclastic mudstone matrix. Thin sections revealed that the carbonate units contain a prominent volcanic matrix composed of disseminated plagioclase laths and abundant chlorite, sericite, and calcite alteration products. Trilobites were recovered from ~2-3-cm-thick fossiliferous grainstone or wackestone horizons within the meterscale carbonate olistoliths, as well as separate beds of fossiliferous grainstone outside the olistoliths.

The Whale Mountain volcanic rocks are prominently exposed where the middle reaches of the Kongakut River cut across the central belt (Fig. 1). They include dark-green basalt and diabase that weather dark olive brown and commonly crop out as fractured pillows (Fig. 4F), massive flows, or minor hypabyssal intrusions (sills and dikes). The basaltic flows typically interfinger with various tuffaceous and volcaniclastic rocks, including lithic and volcanic wacke and conglomerate. The conglomerate is typically clast-supported and contains well-rounded, gravel- to cobble-sized clasts of weathered basalt, diabase, and chert (Fig. 4G).

In thin section, the basalt samples from the central belt display a variety of microtextures (Figs. 5A-5D). Most samples are porphyritic, with textures that range from aphyric (<1% phenocrysts) to highly porphyritic (>10% phenocrysts). Olivine, clinopyroxene, and plagioclase are the dominant phenocrysts, although in some samples, olivine and clinopyroxene are the only phenocrysts present (e.g., 12JT13b; Fig. 5A). Many of the large olivine phenocrysts are crosscut by fractures and have undergone extensive serpentinization and iddingsite alteration, in some cases causing complete replacement of olivine by serpentine and other clay minerals (Fig. 5B). Plagioclase is commonly present as large (~1-4 mm) glomerocrysts forming aggregates with olivine (Fig. 5C). The plagioclase phenocrysts have undergone saussuritization, replacing the plagioclase with an assemblage of cryptocrystalline (<0.1 mm) epidote, clinozoisite, zoisite, and sericite. Amygdules are present in almost all samples and typically compose 1%-5% of the rock volume of each sample; they range from 0.25 to 5 mm in diameter and are semispherical to elongate in shape. The amygdules are typically filled with chlorite group minerals, microcrystalline quartz, calcite, or zeolites (Fig. 5C).

The composition and texture of the groundmass also vary from sample to sample. In some samples, the groundmass is composed of microcrystalline to fine-grained (0.1–1 mm) plagioclase, subhedral Fe- and Ti-oxide minerals, and cryptocrystalline pyroxene or olivine. In other samples, the groundmass is predominantly composed of altered glass and cryptocrystalline to microcrystalline subhedral Fe- and Ti-oxides. When plagioclase microlites are present in the groundmass, they are typically aligned in a moderately to weakly developed trachytic texture (Fig. 5D)

The basaltic flows and volcaniclastic rocks are locally interbedded with a dark-maroon and gray argillite and phyllite, with minor beds of chert, which could be correlative units of the Romanzof formation in the southern belt. The stratigraphic relationships between the various volcanic and carbonate units throughout the central belt are also somewhat uncertain, but their intercalated nature, and the prevalence of volcanic debris within the carbonate units support a cogenetic relationship.

Northern Belt

The northern belt of the allochthon extends from the Malcolm River in northern Yukon to the Ekaluakat River in Alaska (Fig. 1). The stratigraphy of this belt predominantly consists of volcaniclastic and volcanic-rich sandstone units that interfinger with beds of chert, argillite, and black slate (Fig. 2). In Alaska, these units were originally assigned to sequence E of Dutro et al. (1972), and they were subsequently split by Reiser et al. (1980) into three separate Ordovician map units: a "volcaniclastic and volcanic" unit (Ovc), a "black slate" unit (Os), and a "gray phyllite and chert" unit (Opc). On the Yukon side of the international border, these units were mapped as part of a coherent basinal succession of Cambrian–Lower Devonian strata (e.g., Lane,

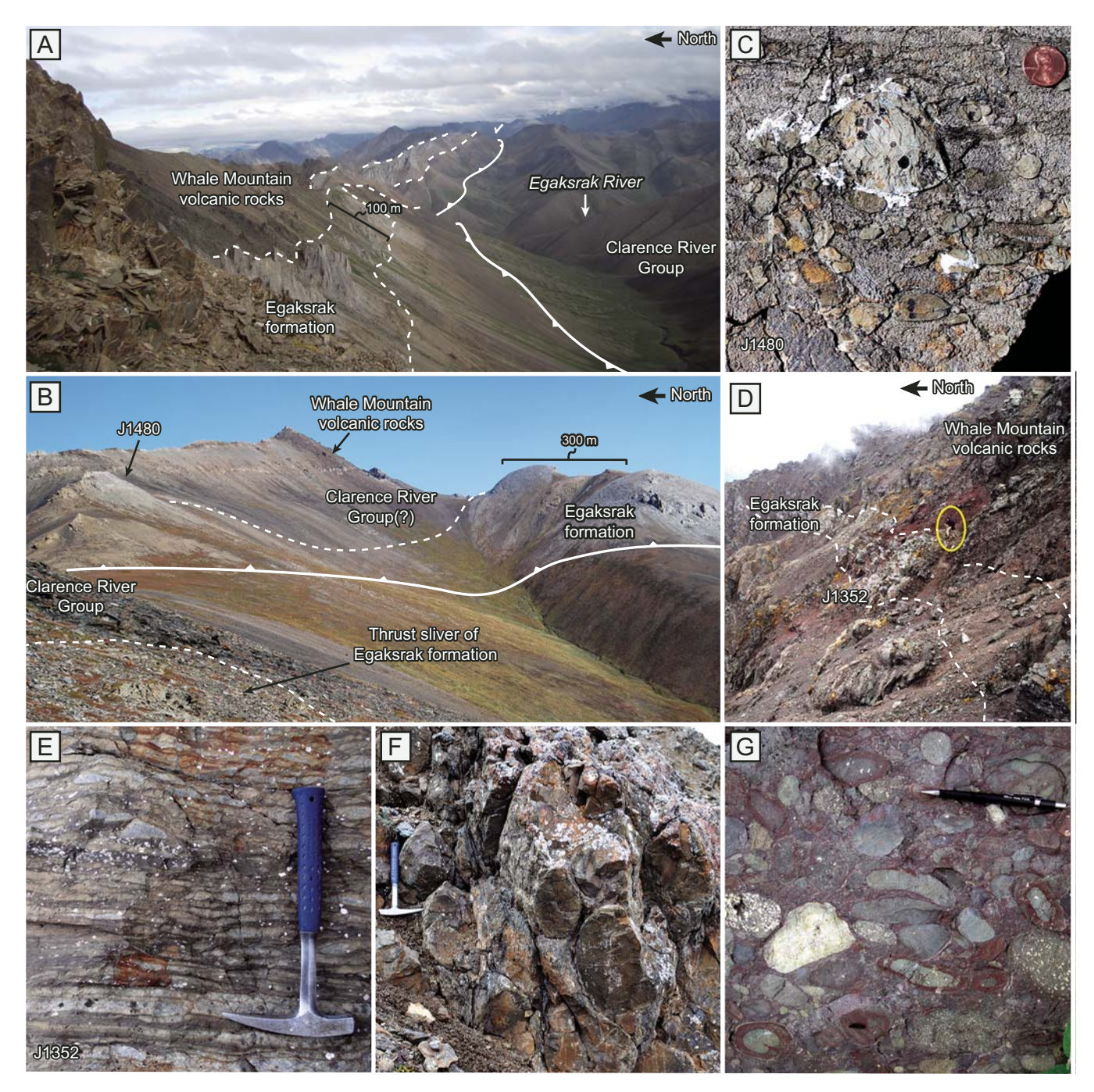


Figure 4. Field images of rocks in the central belt of the Whale Mountain allochthon in the NE Brooks Range, Alaska. (A) Looking east along the southern limb of a synclinal ridge, showing interbedded Whale Mountain volcanic rocks and laminated lime mudstone units of the Egaksrak formation. (B) Looking northeast at the Leffingwell Fork fossil locality (J1480), which shows the Upper Cambrian limestone units above black slate units of the Middle Ordovician–Lower Devonian(?) Clarence River Group, including thrust slivers of Egaksrak carbonate units. (C) Close-up of lime mudstone with abundant pebble- and cobble-sized clasts of basalt; penny for scale is 19 mm across. (D) Looking east at the J1352 fossil location in headwaters of the Malcom River, Yukon; person for scale is circled in yellow and is ~2 m tall. (E) Close-up of ribbon-bedded lime mudstone at the J1352 fossil location; hammer for scale is ~32 cm. (F) Pillow textures preserved within folded basalt flows; hammer for scale is 32 cm long. (G) Close-up of clast-supported conglomerate with well-rounded clast of basalt, diabase, and chert from the Kongakut River, Alaska; pencil for scale is ~15 cm.

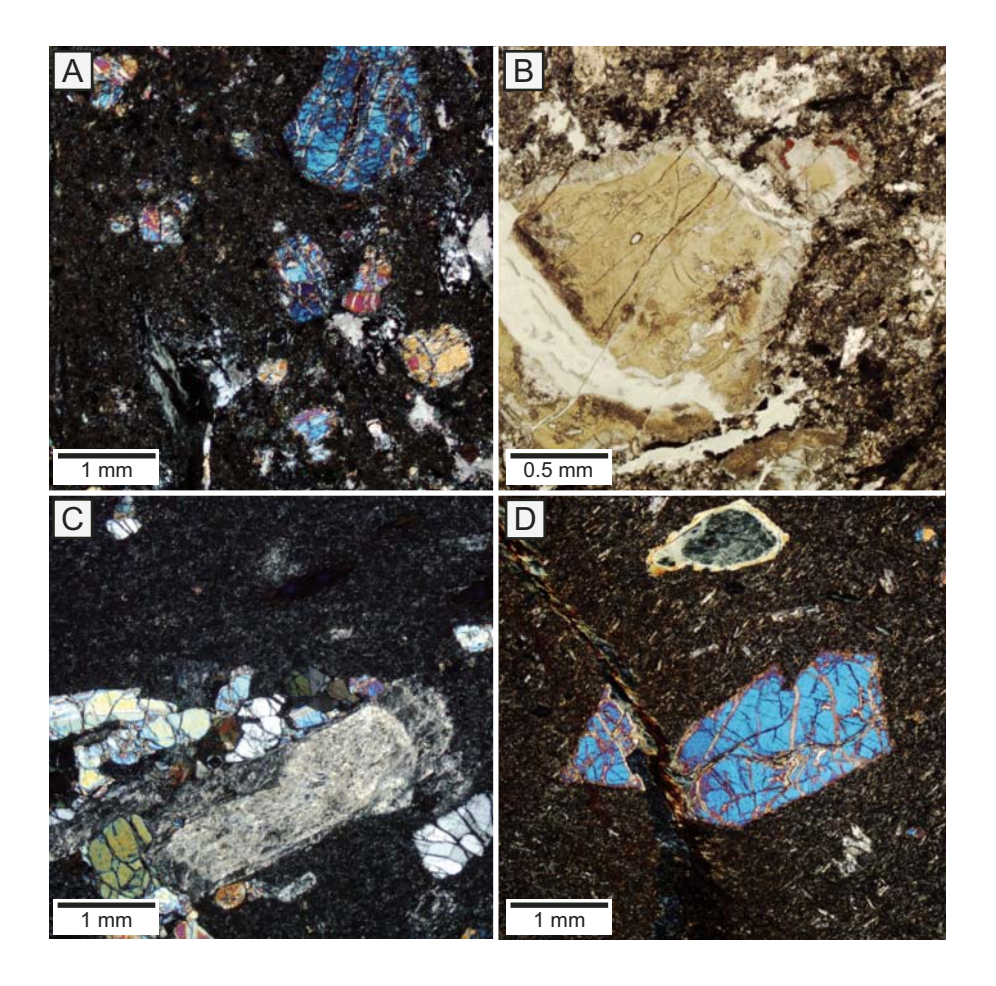


Figure 5. Photomicrographs of the Whale Mountain volcanic rocks. (A) Cross-polarized view of sample 12JT13B, showing fractured olivine phenocrysts in a ground-mass composed of glass and Fe- and Tioxide minerals. (B) Plane-polarized view of sample 12JT20, showing complete iddingsite alteration of an olivine phenocryst. (C) Cross-polarized view of sample 12JT18 showing glomeroporphyritic olivine and plagioclase, sericitization of plagioclase phenocrysts, and chlorite amygdules that have been stretched. (D) Cross-polarized view of sample 20LF13 showing large fractured and altered olivine phenocrysts.

1991; Lane et al., 1995; Lane et al., 2016); however, we tentatively assign these sedimentary and volcanic rocks to a single informal lithostratigraphic unit, which we name the Ekaluakat formation due to its widespread exposure near the Ekaluakat River in Alaska.

Unlike the southern and central belts of the allochthon, the northern belt has a poorly defined base, where discrimination of the sedimentary rocks of the Ekaluakat formation from those of the Clarence River Group is largely hampered by poor exposure and repeated imbrication. However, Reiser et al. (1980) mapped a distinct fault-related breccia unit along the Ekaluakat River that appears to separate volcanic and sedimentary rocks of the Ekaluakat formation from structurally(?) underlying rocks of the Neoproterozoic-Lower Cambrian(?) Firth River Group. Reiser et al. (1980) also reported a ca. 484 Ma K-Ar age on hornblende from a mafic intrusion near the breccia unit. Although we are unsure if the rocks of the Ekaluakat formation are unambiguously correlative with the volcanic and sedimentary rocks of the southern and central belts, this potential tectonic contact is similar to other boundaries with the Whale Mountain allochthon. The top of the Ekaluakat formation is also poorly constrained, because it is either truncated by the

unconformity at the base of the overlying Lower Mississippian Kekiktuk Conglomerate, or it is in thrust contact with older units (Reiser et al., 1980; Lane et al., 1995).

In the summer of 2012, we traversed along a north-trending ridge on the east bank of the lower Kongakut River, which exposes a steeply southward-dipping (~60°-75°) section of Ekaluakat rocks, with the top of the section concealed by the Kekiktuk Conglomerate. Below the unconformity and further north along the ridge, the section contains 0.5-1.5-m-thick beds of dark-brown and massive volcanic-rich pebble conglomerate. Similar outcrops were observed during a 2013 expedition on the Yukon side of the border, where clasts from the conglomerate consist of basalt and minor sedimentary lithics that are moderately rounded and range between 2 and 80 mm in diameter (Fig. 6A).

Further north along the Kongakut River section, the volcanic beds become thinner and more fine grained, and we collected two samples (12JT37 and 12JT39) for thin section and geochemical analysis. The two samples resemble tuffaceous breccia, consisting of a fine- to coarse-grained mixture of volcanogenic minerals, including rounded basalt clasts, loose grains of clinopyroxene and plagioclase, and fine-grained

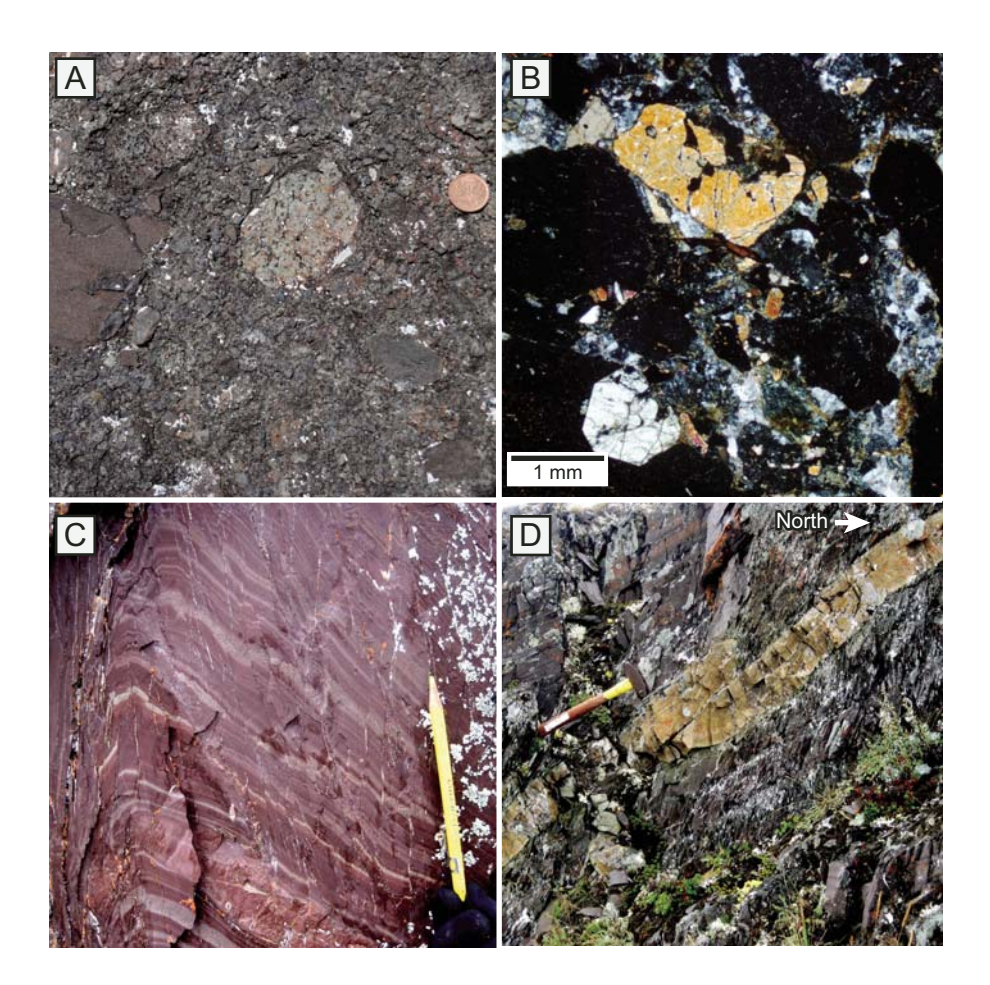


Figure 6. Field images of the Ekaluakat formation from the northern belt of the Whale Mountain allochthon in the NE Brooks Range, Alaska. (A) Close-up taken from volcanic breccia of the Ekaluakat formation exposed in northern Yukon; one-cent piece for scale is 1.9 cm in diameter. (B) Crosspolarized view of sample 12JT39 showing volcanic clast and clinopyroxene grains in a chert(?) and clay matrix. (C) Close-up of folded and laminated maroon argillite, crosscut by steep microshear fractures; pencil for scale is ~13 cm. (D) Photo looking west along the Kongakut River section of the northern belt showing laminated darkmaroon and gray argillite interbedded with a faulted, tan-weathering tuff layer; hammer for scale is ~33 cm.

chert (Fig. 6B). The basalt clasts are moderately porphyritic, containing 5%–10% clinopyroxene (augite) phenocrysts in a glassy to microcrystalline groundmass composed of plagioclase (<0.2 mm) and Fe- and Ti-oxide minerals. The clasts are generally fresh, showing little to no alteration from weathering or metamorphism, but in the surrounding groundmass, low-temperature alteration is common. Calcite, microcrystalline quartz, and clay minerals form veinlets in the groundmass and fill amygdules.

The northern parts of the Kongakut River section expose finely laminated, maroon, green, and dark-gray argillite that is crosscut by a steeply dipping network of microshear fractures that occur in the cores of small folds (Fig. 6C). The argillite is locally interbedded with a distinctive tan and greenish-gray tuff unit (Fig. 6D). A dark-gray, medium- to coarse-grained, volcanic-rich wacke is also occasionally interbedded with the argillite. The wacke consists mostly of reworked volcanic and detrital carbonate grains. Johnson et al. (2016) reported 63 concordant zircon U-Pb ages from this unit (sample 12JT35), 62 of which provided a broad unimodal age population ranging from ca. 602 to 440 Ma and centered at ca. 500 Ma.

ZIRCON U-Pb GEOCHRONOLOGY AND Hf ISOTOPE GEOCHEMISTRY

Zircon U-Pb geochronology and Hf isotope geochemistry from the two volcaniclastic samples (15BJ06 and 13WW23) provide potential constraints on the age and magmatic setting of the volcanic rocks from Whale Mountain allochthon. Standard mineral separation and imaging procedures were followed at the University of Iowa, which included crushing, sieving, water density and magnetic separation, and heavy liquid density separation. The separated zircon grains were mounted in epoxy, ground to expose the grain interiors, and polished prior to cathodoluminescence (CL) and backscattered electron (BSE) imaging using a scanning electron microscope (SEM).

The mounted zircon grains were taken to the University of Arizona LaserChron Center in Tucson, Arizona, to measure the U-Pb and Lu-Hf isotopic ratios by laser ablation–inductively coupled plasma–mass spectrometry (LA-ICP-MS). The CL and BSE images were used to select spot locations for the insitu measurement from each grain in order to avoid inherited cores, complex zoning, or zones of possible metamictization. The U-Pb isotopes were measured first using a 20-µm-diameter

ablation site to determine the age of each grain following the methods of Gehrels et al. (2008). A subset of the measured grains from the same mounts was analyzed for Hf isotope geochemistry using high-resolution-ICP-MS (HR-ICP-MS) and following methods outlined by Gehrels and Pecha (2014). In each Hf isotope analysis, a 40-µm-diameter ablation site was centered over the previously excavated U-Pb analysis pit to help ensure that the initial Hf isotopic composition was measured from the same domain as the U-Pb age. The detailed analytical procedures and filtering methods, along with tables of the individual measurements, are included in the supplemental data material in the GSA Data Repository.¹

U-Pb ages from each of the volcaniclastic samples are shown on the two concordia diagrams in Figures 7A and 7B, which were generated using Isoplot 4.1 software (Ludwig, 2012). Reported uncertainties for each U-Pb age are at the 1σ level and include only measurement errors. A "best age" (see Table DR2) for each grain was selected using a cutoff of 900 Ma from the calculated ²⁰⁶Pb/²³⁸U ages. For zircon grains with ²⁰⁶Pb/²³⁸U ages older than 900 Ma, we used the calculated ²⁰⁷Pb/²⁰⁶Pb ages instead. Several ages were excluded/rejected from the data plots or interpretations because of discordance between the ²⁰⁶Pb/²³⁸U and the ²⁰⁶Pb/²⁰⁷Pb ages calculated for each grain. Grains with >20% discordance were rejected, as were grains with >5% reverse discordance.

U-Pb Geochronological Results

The two analyzed samples were composed of highly sheared and angular volcanic detritus (mostly plagioclase) and volcanic rock fragments set within an altered matrix of sericite and calcite. The southern belt sample (15BJ06) yielded more than 300 grains from the heavy mineral separation procedure. Nineteen of these grains analyzed by LA-ICP-MS yielded spurious isotopic ratios and were thus excluded from further data reduction. Using the CL images, we determined that these grains are not zircon because they lacked measurable luminescence (see GSA Data Repository). The remaining 281 grains consisted of light purple to clear angular grains that ranged from ~50 to 150 µm in length. Seventy-three of these grains showed discordance among the ²⁰⁶Pb/²³⁸U and ²⁰⁶Pb/²⁰⁷Pb ages and were thus excluded from our "best age" filter. An additional five grains were excluded because they yielded ²⁰⁶Pb/²³⁸U ages younger than 200 Ma. These grains showed strong zonation in the CL images (see GSA Data Repository), and we infer that they were a result of sample contamination. The remaining 203 grains yielded ages from ca. 2578 to 354 Ma; however, most of the ages (n = 200) ranged from ca. 544

¹GSA Data Repository Item 2018420, Appendix 2: Detailed description and summary of LA-ICP-MS analytical procedures; Figure DR1: Example CL images of 15BJ06; Table DR1: Sample locations; Table DR2: U-Pb LA-ICP-MS zircon results; and Table DR3: Hf isotopic results, is available at www.geosociety.org/datarepository/2018/, or on request from editing@geosociety.org or Documents Secretary, GSA, P.O. Box 9140, Boulder, CO 80301-9140, USA.

to 473 Ma and constituted a weighted mean age of 512 ± 1.4 Ma (1σ) with a mean square weighted deviation (MSWD) of 0.88 (Fig. 7A). A MSWD of 0.88 is close to 1.0, which implies that the observed scatter in the ages is consistent with precision, and that the analytical precision of the method employed is unable to resolve differences among the age populations (e.g., Wendt and Carl, 1991).

Sample 13WW23 was collected from the eastern edge of the central belt in Yukon at the same location as fossil locality J1352 (Fig. 1). Like sample 15BJ06, 13WW23 is predominately composed of angular volcanic material, and the separated zircon grains are angular and range from ~50 to 150 μ m in length. The sample only yielded seven zircon grains, and one of the grains was excluded from further discussion because of discordance among the $^{206}\text{Pb}/^{238}\text{U}$ and $^{206}\text{Pb}/^{207}\text{Pb}$ ages. The other six grains had ages ranging from ca. 514 to 485 Ma, with a $^{206}\text{Pb}/^{238}\text{U}$ weighted mean age of 504 \pm 11 Ma (Fig. 7B) and a MSWD of 0.65, which could indicate that the observed scatter among the ages is less than that predicted by the analytical uncertainties.

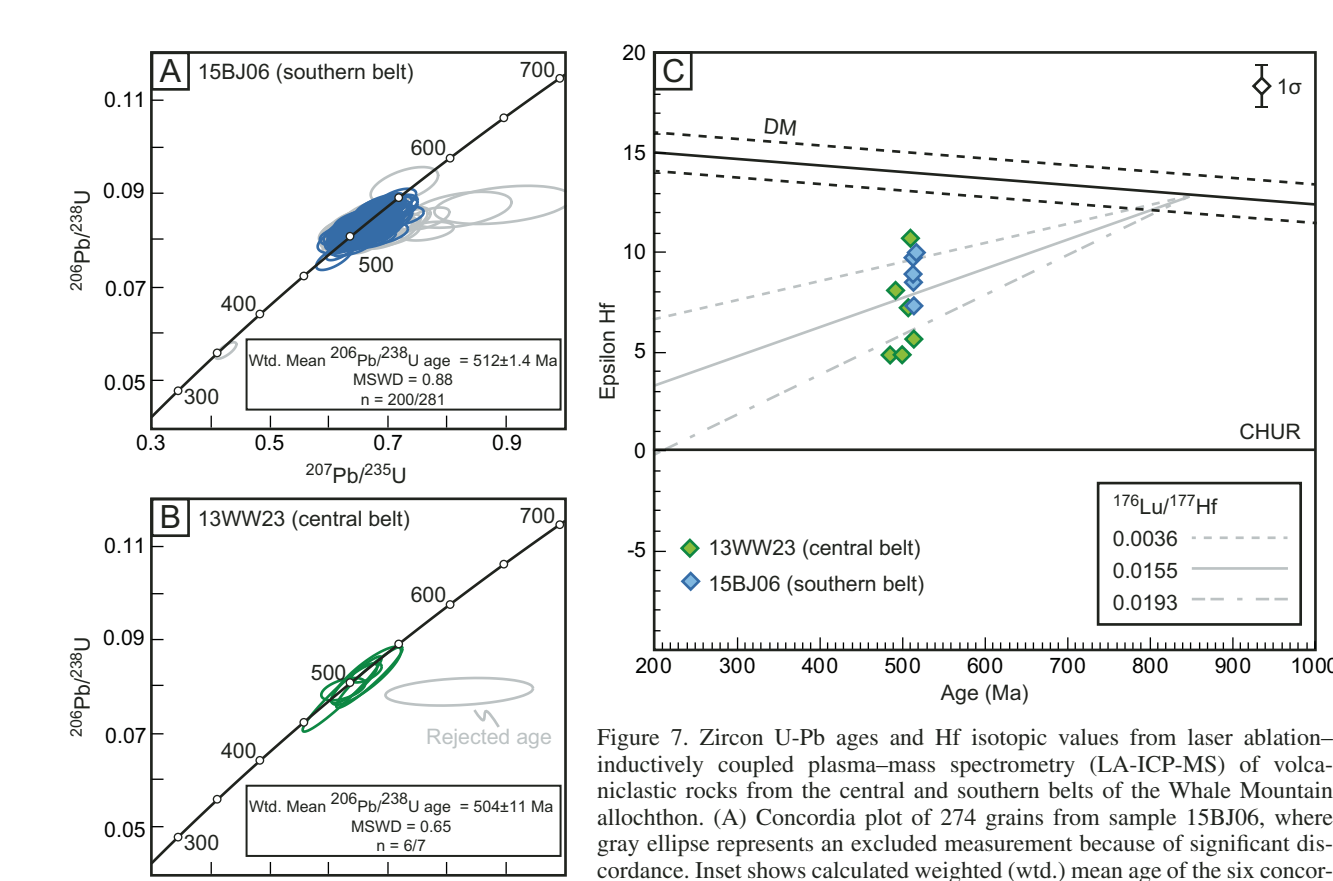
Hf Isotope Geochemistry

Hafnium isotopic measurements were performed on 11 individual grains: five from sample 15BJ06 and six from sample 13WW23. We specifically targeted grains with ages in the 544–475 Ma range because we inferred that those grains would represent the time at which the volcanic rocks erupted. The data are presented on a Hf-evolution diagram (Figs. 7C) that shows $\epsilon_{\rm Hf(f)}$ values at the time of crystallization. The $\epsilon_{\rm Hf(f)}$ values were determined by comparing the measured Hf isotopic values of an individual grain relative to the known Hf values of a chondritic uniform reservoir (CHUR; Bouvier et al., 2008) at the time of crystallization.

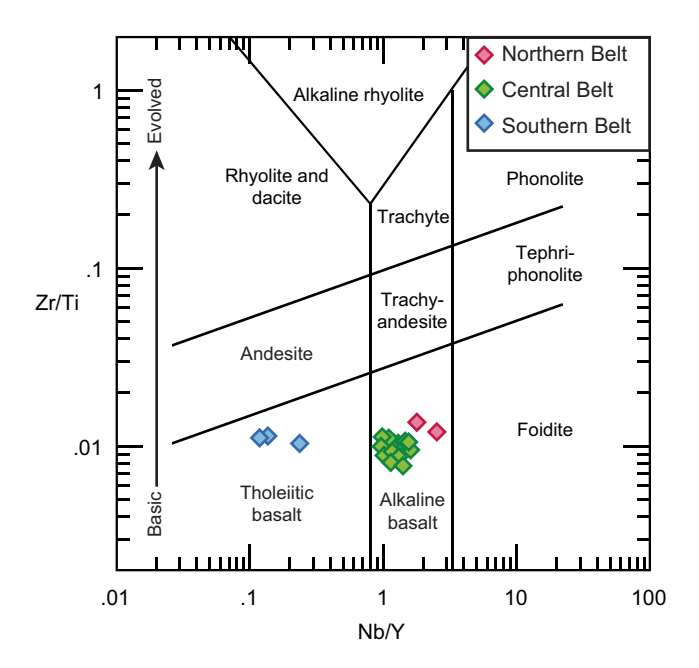
The Hf data from the two samples are similar, with $\epsilon_{\rm Hf(t)}$ values that range from 4.8 to 10.7. These values are considered as intermediate and juvenile in composition because they plot just below the depleted mantle trajectory. Several different interpretations can explain these values. One possible explanation is that the extracted melts from which the zircon grains crystallized were produced by melting of Neoproterozoic crust. This is inferred from the Hf evolution trajectories of felsic crust (gray lines in Fig. 8C), which are based on the average present-day $^{176}\text{Lu}/^{177}\text{Hf}$ ratio of 0.0115 (Vervoort and Patchett, 1996; Vervoort et al., 1999). A second explanation is that melts were derived from the depleted mantle but experienced contamination from enriched sources, such as old (>1000 Ma) crustal rocks or possibly enriched reservoirs in the mantle.

IGNEOUS GEOCHEMISTRY

Twenty-five whole-rock basalt samples were collected from outcrops in the British and Romanzof Mountains of the NE Brooks Range (Fig. 1), including three samples from the southern belt, 20 samples from the central belt, and two samples from



seven grains from sample 13WW23. Inset shows calculated weighted (wtd.) mean age of the six concordant ages. (C) Hf evolution plot showing $\varepsilon_{Hf(t)}$ values for each sample (13WW23 and 15BJ06). The average measurement uncertainty for all analyses (upper right) is shown at the 1σ level. Reference lines on the Hf plot are as follows: DM—depleted mantle, calculated using 176 Hf/ 177 Hf $_0$ = 0.283225 and 176 Lu/ 177 Hf $_0$ = 0.038512 (Vervoort and Blichert-Toft, 1999); CHUR—chondritic uniform reservoir, calculated using 176 Hf/ 177 Hf = 0.282785 and 176 Lu/ 177 Hf = 0.0336 (Bouvier et al., 2008); gray dashed lines show interpreted felsic crustal evolution trajectories assuming present-day ¹⁷⁶Lu/¹⁷⁷Hf = 0.0115 (Vervoort and Patchett, 1996; Vervoort et al., 1999).



the northern belt. The samples were subsequently trimmed to exclude visible alteration and weathering, crushed using a mortar and pestle, and powdered in a SPEX 8515 Shatterbox. The sample powders were shipped to Activation Laboratories LTD (Actlabs) in Ontario, Canada, where they were mixed with a flux of lithium metaborate and lithium tetraborate and fused into glass beads using an induction furnace. The major-element oxides (e.g., SiO₂, MgO, etc.) and a subset of trace elements (Sr, Ba, Sc, V, Y, and Zr) were determined by inductively coupled plasma-optical emission spectrometry (ICP-OES) using a Thermo Jarrell-Ash ENVIRO II ICP or a Varian Vista 735 instrument. The remaining trace elements were determined by ICP-MS using a Perkin Elmer Sciex ELAN 9000 instrument. The calibration of the results was

dant ages. MSWD—mean square of weighted deviates. (B) Concordia plot of

Figure 8. Nb/Y-Zr/Ti discrimination plot of Pearce (1996), where Zr/ Ti ratio is used as an index of differentiation, and Nb/Y is used as an alkalinity index.

0.3

0.5

0.7

²⁰⁷Pb/²³⁵U

0.9

Johnson et al.

TABLE 1. MAJOR-ELEMENT CHEMISTRY OF THE WHALE MOUNTAIN ALLOCHTHON, ALASKA AND YUKON

Sample number	SiO ₂	TiO ₂	Al ₂ O ₃	Fe ₂ O ₃ (T)*	MnO	MgO	CaO	Na ₂ O	K ₂ O	P ₂ O ₅	LOI	Total
Southern belt												
14BJ22	45.02	2.865	15.11	13	0.218	8.5	7.3	2.88	0.25	0.28	4.01	99.44
14BJ24	54.72	1.777	12.58	13.21	0.18	4.28	4.71	3.9	0.4	0.22	4.63	100.6
15BJ08	43.64	3.055	14.25	16.11	0.229	6.57	10.63	2.58	0.13	0.32	3.25	100.8
Central belt												
12JT13B	42.07	1.814	13.03	11.21	0.206	12.21	13.56	0.16	0.001	0.18	6.36	100.8
12JT14	46.72	2.782	14.48	11.81	0.162	6.53	10.96	1.66	0.01	0.32	3.84	99.29
12JT15	46.33	2.336	16.39	9.36	0.234	6.6	11.25	2.14	0.21	0.26	5.53	100.7
12JT16	45.45	3.118	14.47	15.72	0.202	6.54	5.22	3.88	0.02	0.37	4.76	99.74
12JT17	42.87	2.586	15.2	12	0.173	7.97	12.16	1.93	0.03	0.32	4.26	99.48
12JT18	48.02	2.841	16.16	10.22	0.198	8.07	6.18	4.09	0.36	0.32	4.15	100.6
12JT19	49.52	2.749	13.55	11.99	0.141	6.09	10.1	0.51	0.001	0.32	5.74	100.7
12JT20	41.24	1.951	14.56	11.72	0.14	9.89	13.46	0.09	0.001	0.21	5.85	99.13
12JT21	49.91	3.23	13.2	14.44	0.209	5.12	7.63	3.26	0.07	0.32	3.41	100.8
17LF13	48.85	2.789	16	11.33	0.14	6.38	3.31	4.08	0.95	0.31	5.15	99.29
18LF13	54.97	3.373	16.27	7.63	0.064	4.24	2.69	1.87	4.3	0.41	4.14	99.96
19LF13	47.4	2.938	13.88	12.03	0.199	8.2	8.44	3.59	0.46	0.34	3.15	100.6
20LF13	48.78	2.443	13.67	12.53	0.17	8.19	6.85	3.96	0.41	0.27	3.56	100.8
21LF13	49.07	2.721	13.8	11.45	0.158	7.13	7.88	3.98	0.66	0.32	3.74	100.9
22LF13	49.26	3.045	14.59	12.55	0.181	6.45	4.01	4	0.61	0.34	5.06	100.1
23LF13	46.72	3.211	14.43	11.26	0.152	6.75	5.6	3.15	1.12	0.37	6.77	99.51
13MC-062	47.76	2.604	13.35	12.94	0.163	8.21	7.85	4.42	0.06	0.31	3.21	100.9
13MC-063	50.33	2.317	14.98	9.19	0.219	6.51	6.3	5.21	0.06	0.28	4.15	99.56
13MC-065	46.43	2.552	14.5	12.19	0.185	6.91	10.56	3.11	0.21	0.28	2.41	99.35
13JVS-362	46.82	3.066	14.91	13.34	0.181	6.15	9.11	3.69	0.41	0.38	2.11	100.2
Northern belt												
12JT37	39.85	5.199	9.55	15.77	0.202	9.8	10.52	2.27	1.31	0.77	4.41	99.66
12JT39	45.49	4.266	12.06	12.2	0.192	5.45	11.1	4.49	0.3	0.87	4.1	100.5

TABLE 2. TRACE-ELEMENT CHEMISTRY OF THE WHALE MOUNTAIN ALLOCHTHON, ALASKA AND YUKON

Sample number	Rb	Sr	Cs	Ва	Cr	Co	Ni	Cu	Zn	Sc	V	Υ	Zr	Nb	Hf
Southern belt															
14BJ22	5	186	2.3	92	270	50	130	150	100	50	426	47	204	6	5.0
14BJ24	6	156	1.1	51	210	36	100	30	70	37	268	33	126	4	3.1
15BJ08	2	223	< 0.5	62	150	47	60	160	110	43	485	38	191	9	4.5
Central belt															
12JT13B	<2	950	< 0.5	17	980	62	400	90	80	39	256	14	99	17	2.4
12JT14	<2	1341	< 0.5	36	160	40	110	170	100	31	313	22	173	25	4.3
12JT15	4	1307	< 0.5	82	190	45	130	180	80	32	291	16	134	19	3.4
12JT16	<2	191	< 0.5	28	60	43	70	40	110	33	349	25	187	27	4.7
12JT17	<2	515	< 0.5	54	140	44	100	90	90	34	323	20	161	28	4.0
12JT18	7	321	< 0.5	118	190	79	120	380	120	33	322	26	175	26	4.5
12JT19	<2	66	< 0.5	24	130	39	90	80	90	30	291	23	185	25	4.3
12JT20	<2	944	< 0.5	34	800	65	400	110	80	37	260	14	105	17	2.6
12JT21	<2	68	< 0.5	63	30	47	60	60	130	28	417	20	158	28	4.0
17LF13	8	217	1.5	1643	90	42	50	100	110	30	334	21	168	26	4.0
18LF13	53	54	1.6	896	150	97	140	110	160	32	329	25	209	30	5.2
19LF13	4	430	< 0.5	577	190	44	150	40	100	31	322	21	185	32	4.3
20LF13	6	221	3.8	391	220	45	150	20	90	29	304	17	132	22	3.3
21LF13	7	399	1.9	697	230	39	130	30	80	31	307	20	176	29	4.1
22LF13	9	524	4.9	607	150	39	110	170	100	30	328	22	192	28	4.6
23LF13	12	191	8.0	439	190	42	120	30	90	32	310	21	199	33	4.9
13MC-062	<1	160	<0.1	59	490	51	210	30	90	36	337	24	151	26	3.6
13MC-063	<1	203	<0.1	83	160	43	70	30	100	29	265	24	160	24	4.0
13MC-065	2	485	0.4	134	220	47	110	120	90	34	337	23	141	23	3.6
13JVS-362	6	465	0.3	169	60	46	60	50	120	34	389	26	184	30	4.4
Northern belt															
12JT37	22	228	2.5	521	590	56	260	70	140	29	354	27	401	68	9.9
12JT39	6	659	1.0	3357	30	36	100	90	140	23	366	33	361	59	8.4

Note: All measurements are in ppm. Measurements with < before the number indicate that the elemental proportions are below the detection limit of the inductively coupled plasma–mass spectrometer (ICP-MS).

Note: All measurements are in wt%. LOI—loss on ignition.
*All Fe is converted and reported as ferric because oxidation state was not determined prior to heating during LOI measurements.

performed using prepared USGS and CANMET certified standard reference materials.

The major- and trace-element compositions of the basalt samples are given in Tables 1 and 2, with the major-element compositions expressed in weight percent (wt%), and the trace element compositions described in parts per million (ppm). The geochemical data were used to distinguish and classify different volcanic suites from each belt. The low to moderate levels of alteration observed in thin section were supported by the moderate (2–7 wt%) loss on ignition (LOI) values. Alteration likely caused some element mobility, especially for the large ion lithophile elements (LILEs). Several samples had K₂O concentrations that were lower than the ICP-OES detection limits (0.01 wt%), and many of the samples showed large variations in Rb and Ce concentrations. Because of this, most of our classifications and interpretations are based on the relative abundances of incompatible and rare earth elements (REEs), which typically remain stable during alteration and metamorphism (e.g., Winchester and Floyd, 1977; Shervais, 1982; Pearce, 1996).

Geochemical Results

Southern Belt

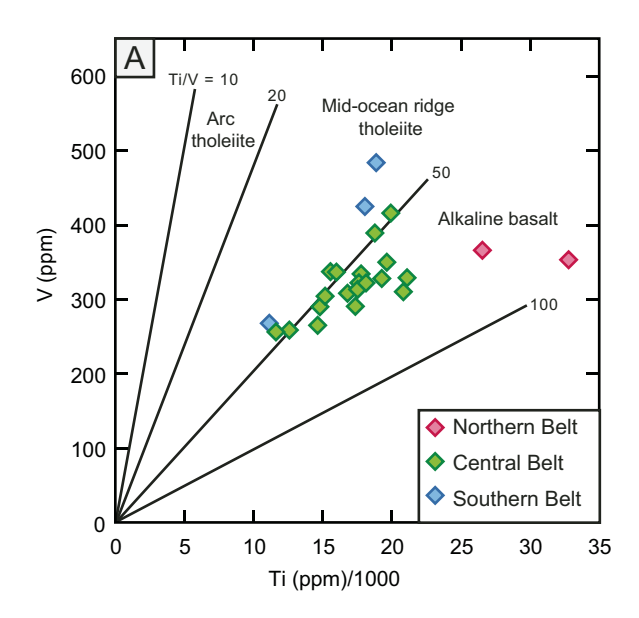
The three samples from the Marsh Fork volcanic rocks of the southern belt have major-element oxide concentrations that resemble average basalt (Table 1), although one sample (14BJ24) has elevated ${\rm SiO}_2$ (~55 wt%) and depleted MgO (~4 wt%) concentrations, resembling andesite rather than basalt. All three samples, however, plot within the tholeitic basalt field on the Nb/Y–Zr/Ti plot (Fig. 8), showing Nb/Y ratios <1 and Zr/Ti ratios ~0.01. On the Ti-V plot (Fig. 9A), the samples fall within the mid-ocean-ridge basalt (MORB) field and have constant Ti/V ratios of ~40. The nearly constant Ti/V ratios among the samples imply that clinopyroxene was not a fractionating melt phase or a refractory mantle phase during the generation of the melt. In support of this assertion, the petrographic work shows that clinopyroxene is only present as an intergranular phase with larger plagioclase (Fig. 3B).

The southern belt samples show pronounced depletions of the most incompatible elements, yielding relatively flat to slightly positive slopes on the normalized variation diagrams (Fig. 10). The samples also show depletions in the high field strength elements Th, U, Nb, Ta, and La, enrichment in the heavy rare earth elements Dy, Yb, Y, and Lu, and relatively flat slopes on the chondritenormalized REE diagram (Fig. 10A). This is supported by the chondrite-normalized La_N/Sm_N ratios, which range from 0.6 to 1.2, representing the lowest ratios among all the samples in the data set.

Central Belt

The 20 Whale Mountain volcanic samples collected from the central belt show significant variation among most major-element

———	Th	U	La	Ce	Pr	Nd	Sm	Eu	Gd	Tb	Dy	Но	Er	Yb	Lu	Sample number	
0.5		0.00		04.5	4.40	04.7	7.00	0.50	0.70	4.50	0.50	4.00	5 40	5 40	0.70	Southern belt	
0.5	0.7	0.20	7.9	24.5	4.13	21.7	7.30	2.56	8.70	1.50	9.50	1.90	5.40	5.10	0.76	14BJ22	
0.3	0.4	< 0.1	4.8	15.0	2.49	13.8	4.80	1.63	5.80	1.00	6.50	1.30	3.80	3.70	0.55	14BJ24	
0.7	8.0	0.30	11.0	28.2	4.16	19.5	5.90	2.31	7.00	1.30	7.70	1.50	4.30	4.00	0.59	15BJ08	
																Central belt	
1.2	1.2	0.40	14.6	33.0	4.18	17.3	3.80	1.39	3.80	0.60	3.10	0.60	1.50	1.20	0.18	12JT13B	
1.8	2.1	0.60	22.8	52.8	6.56	27.6	6.30	2.29	5.90	1.00	5.00	0.90	2.50	2.00	0.29	12JT14	
1.4	1.6	0.40	15.9	38.6	4.96	20.6	4.70	1.83	4.60	0.70	3.60	0.70	1.70	1.30	0.19	12JT15	
2.0	2.2	0.50	24.0	54.6	7.00	29.0	6.90	2.39	6.90	1.10	5.90	1.10	2.90	2.20	0.31	12JT16	
2.1	2.2	0.60	23.9	55.3	6.79	27.9	6.00	2.06	5.50	0.90	4.70	0.80	2.20	1.70	0.24	12JT17	
1.8	2.1	0.50	18.9	46.4	5.85	24.6	5.90	2.02	5.60	1.00	5.60	1.10	2.90	2.50	0.38	12JT18	
1.8	2.0	0.50	21.7	51.3	6.44	26.4	6.20	2.05	6.00	0.90	5.10	0.90	2.50	1.90	0.26	12JT19	
1.2	1.3	0.40	16.1	36.0	4.33	17.3	3.90	1.56	3.80	0.60	3.30	0.60	1.60	1.20	0.17	12JT20	
2.0	2.2	0.70	23.3	52.5	6.44	26.4	6.00	2.10	5.60	0.90	4.80	0.90	2.30	1.80	0.25	12JT21	
1.8	2.0	0.60	20.8	48.7	6.11	25.2	6.00	2.34	6.00	0.90	4.80	0.90	2.30	1.70	0.24	17LF13	
2.2	2.5	0.60	24.5	58.7	7.08	29.3	6.50	2.02	5.70	0.90	5.00	0.90	2.50	2.00	0.30	18LF13	
2.2	2.4	0.80	26.6	59.5	7.14	28.7	6.40	2.10	5.90	0.90	4.80	0.90	2.30	1.70	0.24	19LF13	
1.5	1.6	0.50	17.5	41.6	5.27	21.9	4.80	1.81	4.70	0.70	3.80	0.70	1.80	1.40	0.21	20LF13	
2.1	2.2	0.70	24.5	57.3	6.98	28.5	6.10	2.16	5.80	0.90	4.60	0.80	2.20	1.80	0.26	21LF13	
2.0	2.3	0.70	23.2	56.2	7.13	31.0	6.90	2.48	6.40	1.00	5.00	0.90	2.30	1.70	0.23	22LF13	
2.4	2.5	0.70	20.9	52.0	6.72	29.1	6.50	2.30	6.00	1.00	5.00	0.90	2.40	1.80	0.24	23LF13	
1.6	1.6	0.42	21.0	46.0	6.13	23.1	5.92	1.86	5.27	0.81	4.62	0.84	2.23	1.93	0.27	13MC-062	
1.8	2.0	0.64	16.9	41.0	5.60	24.5	5.38	1.79	5.06	0.80	4.44	0.80	2.22	1.81	0.26	13MC-063	
1.8	1.5	0.47	15.7	36.9	5.02	20.6	5.41	1.84	5.14	0.81	4.27	0.77	2.08	1.81	0.25	13MC-065	
2.0	2.0	0.45	22.8	51.6	6.94	27.2	6.64	2.19	6.09	0.97	5.19	0.90	2.38	2.04	0.29	13JVS-362	
																Northern belt	
4.6	4.6	1.30	51.5	119.0	14.70	59.6	12.60	4.07	10.70	1.50	6.90	1.10	2.70	1.80	0.26	12JT37	
3.9	5.0	1.60	55.4	123.0	14.80	60.5	12.40	3.86	10.90	1.50	7.50	1.30	3.20	2.30	0.31	12JT39	



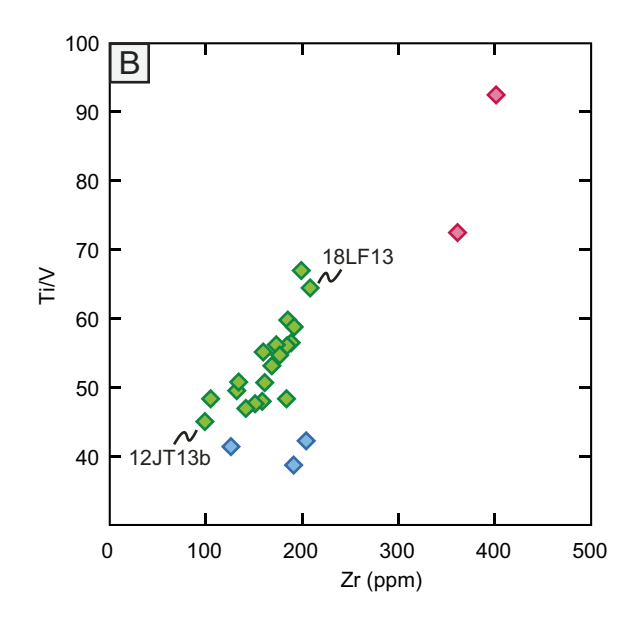


Figure 9. (A) Ti-V plot is after Shervais (1982) showing the fields of low-Ti island-arc tholeiite, island-arc tholeiite, mid-ocean-ridge tholeiite (includes back-arc basin basalt), and alkaline basalt. Solid lines represent constant Ti/V ratios of 10, 20, 50, and 100. (B) Zr-Ti/V plot showing the changes in the Ti/V ratio (controlled by clinopyroxene fractionation) with respect to Zr (a commonly used differentiation index for altered basalt).

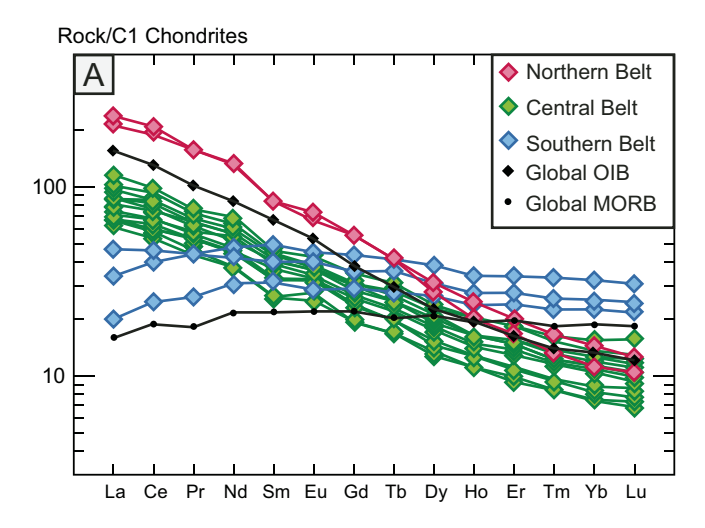
compositions (Table 1), but they are all within typical compositions of basalt. In general, correlation among element pairs is weak, but MgO, which is a common index of differentiation in basalts, is weakly correlated with SiO₂, TiO₂, CaO, and P₂O₅. All the samples from the central belt plot within the alkaline basalt field on the Nb/Y-Zr/Ti plot (Fig. 8) and have Nb/Y ratios that are generally >1. On the Ti-V discrimination plot (Fig. 9A), the samples plot along a linear trend that crosses the 50 Ti/V ratio line at a low angle. This is likely an effect of clinopyroxene fractionation, which causes an increase in the Ti/V ratio as the melt evolves because clinopyroxene preferentially takes on V³⁺ over Ti during crystallization. This is supported by an increase in the Ti/V ratio with respect to Zr concentration (Fig. 9B).

Much of the intrasample variation for central belt samples can be explained by crystal fractionation. Using Zr, another common fractionation index, sample 18LF13, which has the highest concentration of Zr (209 ppm) among the suite, plots at the extreme end of the evolution trend line on the Zr-Ti/V plot (Fig. 9B). In thin section, sample 18LF13 shows almost no recognizable primary phenocrysts, which is likely due to the extensive sericite alteration of plagioclase. Remnants of olivine or clinopyroxene are also absent. At the other end of the evolution trend line, two samples (12JT13b and 12JT20) have low Zr concentrations (<110 ppm) and low Ti/V ratios, which could be the result of little to no fractionation of clinopyroxene. The two samples are distinguished by high concentrations of MgO (>10%) and high concentrations of the compatible trace elements Ni (400 ppm each) and Cr (>800 ppm). This, along with the high abundances of olivine phenocrysts in thin section (Figs. 5A and 5B), favors classification of these two samples as picrites, which could have formed by the accumulation of olivine in a fractionating magma chamber. Samples with more intermediate compositions (Zr = 140–190 ppm) typically show a greater variety of phenocrysts, including clinopyroxene and plagioclase. In some cases, olivine occurs as inclusions within larger plagioclase phenocrysts (Fig. 5C), suggesting that plagioclase crystallized after olivine.

The normalized variation diagrams (Fig. 10) support incompatible element enrichment. The steep negative slopes on the REE diagram (Fig. 10A), along with the 1.8–2.6 La_N/Sm_N ratios, indicate that partitioning of the most incompatible REEs into the melt occurred by low degrees of partial melting or by melting of an enriched mantle source. In the pyrolite-normalized diagram (Fig. 10B), the slopes drastically drop off after Ti due to the low concentrations of Dy, Y, Yb, and Lu. This is likely an indication of refractory garnet in the mantle source, because these elements, although highly incompatible with most minerals, are strongly partitioned into garnet and withheld from the melt (see Discussion section).

Northern Belt

The two volcanic samples from the Ekaluakat formation (12JT37 and 12JT38) collected from the northern belt are characterized by high concentrations of incompatible elements. Both samples show elevated concentrations of ${\rm TiO_2}$ (>4 wt%), ${\rm P_2O_5}$ (>0.75 wt%), and Zr (>350 ppm). Additionally, the two samples have noticeably lower concentrations of ${\rm Al_2O_3}$ (9.55 and 12.06 wt%) and ${\rm SiO_2}$ (39.85 and 45.49 wt%) but show a wide range in MgO concentrations (5.45 and 9.8 wt%). Both samples plot within the alkaline basalt fields on the Zr/Ti-Nb/Y plot (Fig. 8) of Pearce (1996) and the Ti-V plot (Fig. 9) of Shervais (1982).



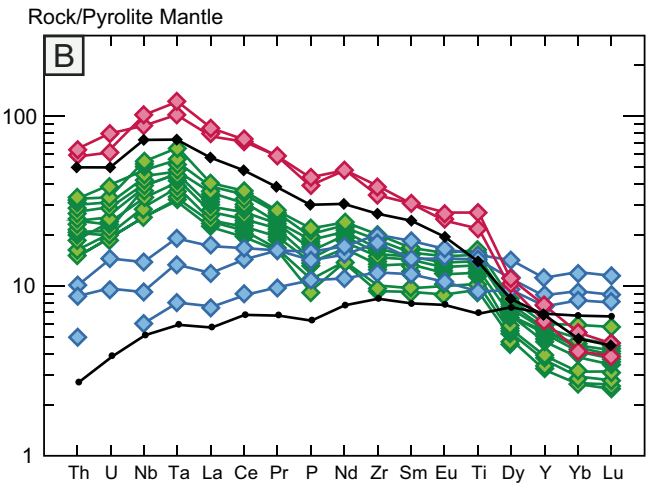


Figure 10. Trace-element variation diagrams. (A) Rare earth elements (REE) normalized to average C1 chondrite compositions from McDonough and Sun (1995). (B) Selected trace-element variations that are normalized to average pyrolite mantle compositions of McDonough and Sun (1995). OIB—oceanic-island basalt; MORB—mid-ocean-ridge basalt.

The significant differences between the two Ti/V ratios, 92.5 for 12JT37 and 72.5 for 12JT39, could be caused by the fractionation of clinopyroxene. Like the central belt samples, the northern belt samples have steep negative slopes on the normalized variation diagrams (Fig. 10), although the northern belt samples show even greater incompatible element enrichment. They have La_N/Sm_N ratios >2.5 and low concentrations of Dy, Y, Yb, and Lu, reflecting the signature of refractory garnet in the mantle source.

PALEONTOLOGY

Dutro et al. (1972) were the first to report Cambrian fossils from the rocks here included in the Whale Mountain allochthon. From exposures of their sequence along the Marsh Fork of the Canning River (Fig. 1), they recovered a trilobite fauna from their "volcanic and carbonate member," strata assigned here to the Egaksrak formation. The trilobites from the Marsh Fork locality were assigned without reservation to the genus *Olenellus*, which confirmed an early Cambrian age and "North American affinities" for these rocks of the southern belt. A second collection, recovered from exposures of the same member near the Leffingwell Fork of the Aichilik River in the central belt, contained trilobites, agnostoid arthropods, and calcitic brachiopods. It also was interpreted as a "North American" fauna, but of late Cambrian age. Both the continental affinity and the age were based on identification of one trilobite in the collection as *Saratogia*. Here, we detail the findings from two new fossil localities and a resampled collection from the Leffingwell Fork locality of Dutro et al. (1972).

Fossil Locality J1475 (Southern Belt)

The Marsh Fork locality was not resampled in our study, but reconnaissance sampling did yield a new fossil locality near the eastern end of the southern belt in the eastern Romanzof Mountains (Figs. 1 and 3A). The faunal collection from this locality, designated J1475, includes at least three agnostoid arthropod species, four or five trilobite species, and phosphatic brachiopods. The agnostoids and trilobites, illustrated in Figure 11, are identified as:

- (1) Pseudagnostus aff. P. parvus Shergold, 1980;
- (2) Pseudagnostus josepha?;
- (3) Neoagnostus? sp.;
- (4) Aplotaspis new species;
- (5) Stenopilus? sp.;
- (6) genus species indeterminate 75A;
- (7) genus species indeterminate 75B; and
- (8) genus species indeterminate 75C.

Details on the morphology and taxonomic assignments are provided in Appendix 1. It is unknown whether genus species indeterminate (gen. sp. indet.) 75C is the pygidium of gen. sp. indet. 75A, gen. sp. indet. 75B, or a fifth trilobite species. The agnostoids and trilobites confirm an age significantly younger than the Marsh Fork fauna and suggests that some of the Egaksrak units in the southern belt are assigned to the upper Cambrian (Furongian Series), although an uppermost middle Cambrian assignment (Guzhangian Stage of the Miaolingian Series) cannot be ruled out entirely.

Fossil Locality J1480 (Central Belt)

The exposures at the Leffingwell Fork locality were resampled in 2014. The new collection, referred to here as J1480, significantly expanded the number of trilobite and agnostoid specimens available to critically evaluate the taxonomic assignments of Dutro et al. (1972). One agnostoid and six trilobites are represented (Fig. 12), including:

- (1) Micragnostus sp.;
- (2) Plethopeltis? sp.;

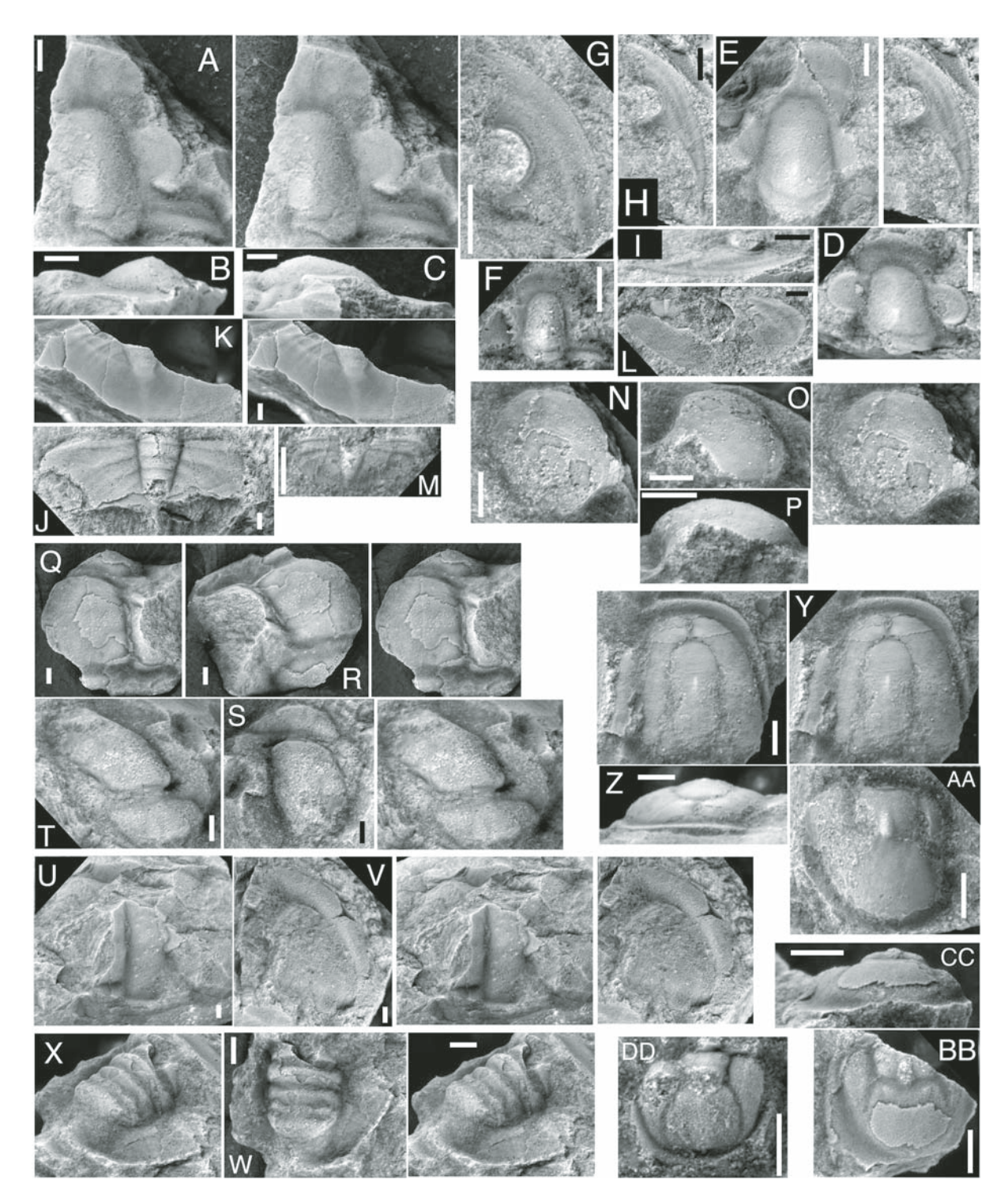


Figure 11. Trilobites and agnostoid arthropods from the Egaksrak formation at locality J1475. View is dorsal (palpebral for cranidia) unless indicated otherwise. White or black scale bar in each photo is ~1 mm in length. A–M: *Aplotaspis* new species; (A–C) dorsal stereopair, anterior, and lateral views of large cranidium, CM59287; (D–F) small CM59288, medium CM59289, and very small CM59290 cranidia; (G) large, fragmentary librigena, CM59291; (H–I) stereopair and exterior view of small librigena, CM59292; (J) large, fragmentary pygidium, CM59293; (K) stereopair of large, fragmentary pygidium CM59294; (L) small, fragmentary pygidium CM59295; (M) very small pygidium CM59296. N–P: *Stenopilus*? sp., dorsal stereopair, anterior oblique, and lateral views of fragmentary small cranidium CM59297. Q–T: Genus species indeterminate 75A, fragmentary large cranidia; (Q–R) dorsal stereopair and anterior oblique views of CM59298; (S–T) dorsal view and anterior-oblique stereopair of CM59299. U–V: Genus species indeterminate 75B; (U) stereopair of large, fragmentary cranidium CM59300; (V) stereopair of large, fragmentary librigena CM59301. W–X: Genus species indeterminate 75C, dorsal and posterior oblique stereopair of fragmentary medium pygidium CM59302. Y–AA: *Pseudagnostus* cf. *P. parvus*; (Y–Z) dorsal stereopair and anterior view of fragmentary large cephalon CM59303; (AA) fragmentary large pygidium CM59304. BB–CC: *Neoagnostus*? sp.; dorsal and posterior views of fragmentary small pygidium CM59305. DD: *Pseudagnostus josepha*?, fragmentary very small pygidium CM59306.



Figure 12. Trilobites and agnostoid arthropods from the Egaksrak formation at locality J1480. View is dorsal (palpebral for cranidia) unless indicated otherwise. White or black scale bar in each photo is ~1 mm in length. A–D: Idahoiid new genus new species 1; (A–C) dorsal, anterior oblique, and anterior views of cranidium CM59307; (D) large librigena CM59308. E–J: Idahoiid new genus new species 2; (E) stereopair of medium cranidium CM59309; (F–G) dorsal view and anterior oblique stereopair of medium cranidium CM59310; (H–I) dorsal and anterior oblique views of small cranidium CM59311; (J) large librigena CM59312. K–L: Genus species indeterminate 80B, dorsal stereopair and anterior oblique view of medium cranidium CM59320. M–Q: idahoiid pygidium 2; (M–N) dorsal stereopair and posterior oblique view of medium pygidium CM59314; (O–Q) dorsal, posterior, and lateral views of small pygidium CM59315. R–S: Idahoiid pygidium 1, stereopair and posterior view of large pygidium CM59313. T–W: *Plethopeltis*? sp.; (T–U) dorsal and anterior oblique views of large cranidium CM59316; (V–W) dorsal and lateral views of medium cranidium CM59317. X–Z: Genus species indeterminate 80A; dorsal, anterior oblique, and anterior views of large cranidium CM59318. AA–CC: Genus species indeterminate 80C; dorsal, lateral, and posterior views of fragmentary medium pygidium CM59321. DD–GG: *Micragnostus* sp.; (DD) stereopair of medium cephalon CM59322; (EE) stereopair of medium pygidium CM59323; (FF–GG) dorsal and lateral views of medium pygidium CM59324.

- (3) idahoiid new genus, new species 1;
- (4) idahoiid new genus, new species 2;
- (5) idahoiid?, genus and species indeterminate;
- (6) genus species indeterminate 80A; and
- (7) genus species indeterminate 80B.

The dominance of the fauna by idahoiids, and the similarity of the agnostoid species to specimens of *Microagnostus chiushuensis* (Kobayashi) illustrated by Westrop (1995) from lower Sunwaptan strata in northwestern Canada support the "mid-Franconian" age assigned to this fauna by Dutro et al. (1972). In modern terms, this equates to the mid-Furongian (Jiangshanian Stage). The idahoiids also link the fauna to Laurentia, but the absence of *Saratogia* and several other genera that occur in most *Saratogia* or *Idahoia* zone faunas across North America (see Discussion) suggests a paleogeographic location somewhat removed from the Laurentian platform itself.

Fossil Locality J1352 (Central Belt)

A new fossil locality (J1352) in the central belt, ~70 km along strike from the Leffingwell Fork locality, yielded a sizable collection (127 specimens) of trilobites and agnostoids. This collection is the most unequivocally synvolcanic sample extracted from the Egaksrak formation. Unlike J1480, which was collected from a carbonate megablock within the mélange at the base of the central belt (Fig. 4B), J1352 was recovered from an interval dominated by thinly laminated volcaniclastic wackestone and lime mudstone, interstratified with pillow basalt and volcaniclastic strata (Fig. 4C). The fossils were recovered from thin lenses and laminae of bioclastic grainstone (Fig. 4D), which attest to a shallow environment of deposition, as does the scarcity of agnostoids, which account for only 4 of the 127 specimens. The following taxa are represented and illustrated in Figure 13:

- (1) agnostoid genus species indeterminate;
- (2) Cheilocephalus? sp.;
- (3) genus species indeterminate 52A;
- (4) genus species indeterminate 52B;
- (5) genus species indeterminate 52C;
- (6) genus species indeterminate 52D;
- (7) genus species indeterminate 52E; and
- (8) genus species indeterminate 52F.

The fauna is assigned an early Furongian age (Paibian Stage) on the presence of a single cranidium with granular texture assigned with slight reservation to *Cheilocephalus* (see Appendix 1). The presence of that genus suggests a linkage to Laurentia, although there have been a few reports of the genus from non-Laurentian successions in Siberia and North China (Westrop et al., 2008).

DISCUSSION

Age of the Whale Mountain Allochthon

The presence of *Olenellus* in the Egaksrak formation at the Marsh Fork locality (Dutro et al., 1972) assigns those strata to

the Dyeran Stage of Laurentia (global Series 2; Fig. 14), confirming that extrusion of lavas in the southern belt had begun prior to the end of the early Cambrian (ca. 509 Ma; Gradstein et al., 2012). This is supported by the ca. 512 Ma weighted average zircon U-Pb age from the southern belt volcaniclastic sample 15BJ06 (Fig. 7A). The agnostoids and trilobites in collection J1475, however, assign other carbonate rocks of the southern belt to the upper Cambrian (Furongian Series). The presence of *Pseudagnostus* confirms that the collection is no older than Guzhangian (Miaolingian Series). The lowest occurrences of that genus reported from several continents (Shergold et al., 1990; Peng and Robison, 2000; Varlamov et al., 2006) all lie above the first appearance datum (FAD) of *Lejopyge laevigata*, the appearance of which marks the base of the Guzhangian Stage (ca. 500 Ma; Gradstein et al., 2012).

At the species level, the trilobites and agnostoids in J1475 more closely resemble younger species from Paibian to lower Jiangshanian strata, suggesting that the fauna is Furongian rather than Guzhangian. As noted in the detailed species comparisons provided in Appendix 1, Aplotaspis n. sp. is most similar to Aplotaspis erugata in the Idamean Stage (mid-Paibian) of Australia (Henderson, 1976), and it also resembles Aplotaspis caelata from the Jiangshanian Plicatolina perlata Zone of Siberia (Lazarenko et al., 2006) in pygidial morphology. The only evidence that J1475 could be younger than Jiangshanian, and instead represents Stage 10, is the tentative assignment of a single, poorly preserved cranidium (Figs. 11N–11P) to the upper Sunwaptan genus Stenopilus. That assignment is far from certain, however, and it would conflict with the stratigraphic ranges established for Aplotaspis and the two species of Pseudagnostus that the agnostoids in J1475 most closely resemble (Pseudagnostus josepha and Pseudagnostus parvus), the youngest reported occurrences of which are from uppermost Jiangshanian (lower Sunwaptan Taenicephalus zone or equivalent) strata (Shergold, 1980; Westrop, 1995; Lazarenko et al., 2006; Chatterton and Gibb, 2016). Accordingly, the carbonate rocks containing the J1475 locality are assigned to either the Paibian or Jiangshanian, indicating that the volcanism in the southern belt continued through ca. 497 Ma, the approximate age determined for the base of the Paibian Stage (Gradstein et al., 2012).

The age constraints of the Romanzof formation are provided by a collection of biserial graptolites that Moore and Churkin (1984) recovered from a succession of argillite and chert (Romanzof formation) along the Canning River in Alaska. The collection included the genera *Climacograptus*, *Retiograptus*, and *Didymograptus*, which broadly occur in Lower–Middle Ordovician strata throughout parts of North America, Europe, and Asia (e.g., Jackson, 1964). The detrital zircon ages from a lithic- and volcanic-rich sandstone unit of the Romanzof formation suggest a ca. 452 Ma maximum depositional age (Strauss et al., this volume, Chapter 23), expanding the age constraints of the southern belt to potentially record a 60 m.y. history that ranges from the early Cambrian (ca. 512 Ma) to the Late Ordovician (ca. 452 Ma).



Figure 13. Trilobites from the Egaksrak formation at locality J1352. View is dorsal (palpebral for cranidia) unless indicated otherwise. White or black scale bar in each photo is ~1 mm in length. A–D: *Cheilocephalus?* sp.; (A–C) dorsal and lateral views, and anterior oblique stereopair of medium cranidium CM59325; (D) posterior-dorsal view of right posterolateral projection showing "shoulder." E–H: Genus species indeterminate 52A; (E–G) dorsal stereopair, lateral, and anterior views of medium cranidium CM59326; (H) fragmentary medium librigena CM59327. I–N: Genus species indeterminate 52B; (I–K) dorsal, anterior, and lateral views of medium, slightly crushed cranidium CM59328; (L) small cranidium CM59329; (M–N) dorsal and exterior views of large librigena CM59330. O–V: Genus species indeterminate 52C; (O–P) dorsal and anterior oblique views of medium cranidium CM59331; (Q) medium cranidium CM59332; (R–S) dorsal and exterior views of large librigena CM59333; (T–V) dorsal, posterior, and lateral views of medium pygidium CM59334. W–Y: Genus species indeterminate 52D, dorsal, anterior, and lateral views of medium cranidium CM59335. Z–AA: Genus species indeterminate 52E, dorsal and exterior views of large librigena CM59336. BB–CC: Genus species indeterminate 52F, dorsal and exterior views of fragmentary medium librigena CM59337. DD–EE: Agnostoid genus species indeterminate, dorsal and lateral views of small cephalon CM59338.

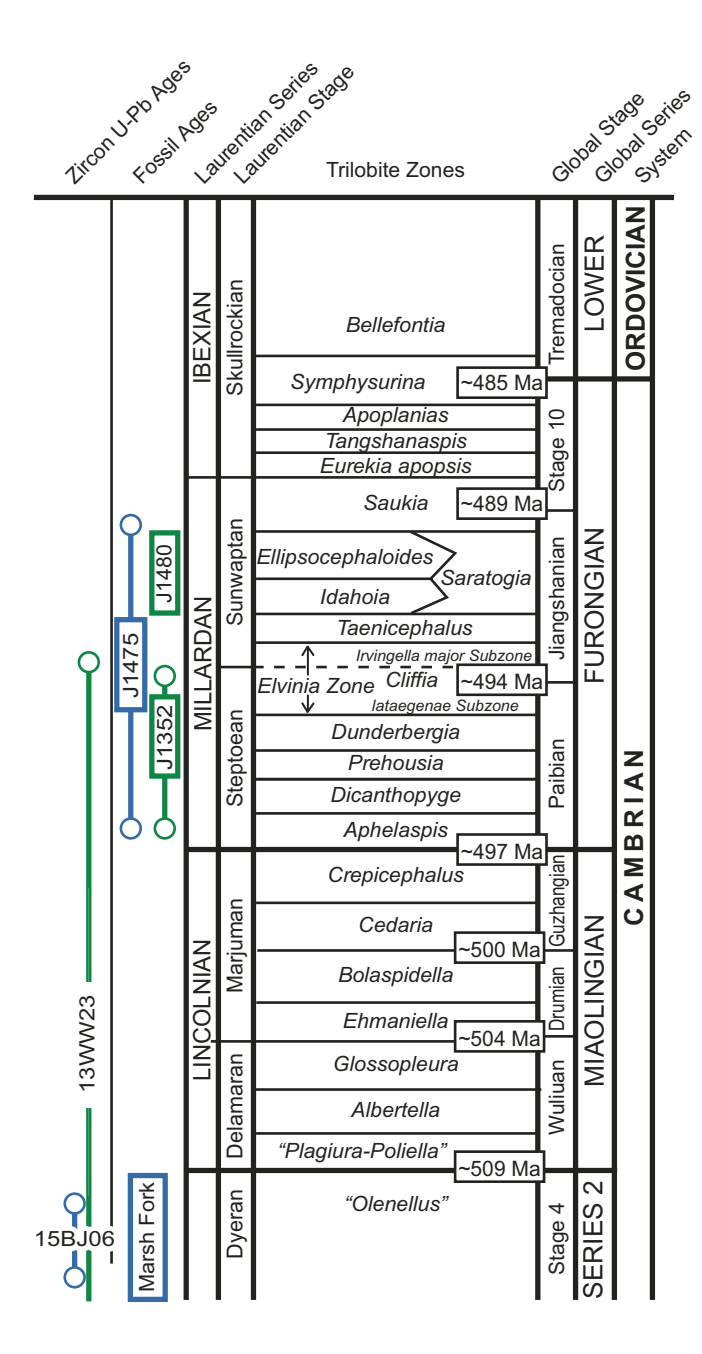


Figure 14. Chronostratigraphic chart showing probable positions of faunal and zircon collections from the Whale Mountain allochthon within the succession of upper Cambrian trilobite-based biochronozones, series, and stages established for Laurentia, and their relationship to global chronostratigraphic units (right-most columns; after Taylor et al., 2012). Numerical ages for the global stages are from Gradstein et al. (2012). Colors are used to differentiate southern belt collections (blue) from central belt collections (green). Colored rectangles for fossil collections depict probable ranges; possible ranges are shown with colored lines and white dots. Estimated ranges for the zircon U-Pb ages were taken from uncertainties depicted in the weighted average age from each sample (Fig. 7).

The rocks of the central belt span a much narrower range in age than those from the southern belt. The two faunas recovered from the Egaksrak formation are assigned to the Furongian, with the trilobites and agnostoid from the Leffingwell Fork locality (J1480) indicating a Jiangshanian age, and the probable *Chei*locephalus in the new collection (J1352) placing it in the Paibian Stage or lowermost Jiangshanian Stage (Fig. 14). Despite reassignment of the agnostoid and idahoiid trilobites reported by Dutro et al. (1972) from the Leffingwell Fork locality to different genera (see Appendix 1), the new information provided by collection J1480 confirms their assessment of the fauna as "Franconian" (now lower Sunwaptan) in age. Like coeval faunas assigned to the Saratogia or Idahoia zones in various locations across North America, J1480 is dominated by idahoiid species. The close resemblance of *Micragnostus* sp. to specimens of *M*. chiushuensis illustrated by Westrop (1995) from the lower Sunwaptan Noelaspis jeffreyi fauna in the Rabbitkettle Formation of northwestern Canada reinforces this correlation.

The uniqueness of the fauna from locality J1352 makes correlation with previously described faunas difficult; however, the one small cranidium identified as *Cheilocephalus*? sp. probably does represent that primarily Steptoean genus. The generic assignment is tentative only because no pygidium or librigena is available to fortify it. *Cheilocephalus* is widely distributed across Laurentia in strata of Steptoean (Paibian) age, with a single occurrence in deep-water deposits of uppermost Marjuman (Guzhangian) age in Newfoundland (Westrop et al., 2008). However, that older species of *Cheilocephalus* lacks the granular sculpture displayed by the cranidium in J1352.

The Furongian fossil age of the central belt carbonate rocks is supported by the ca. 504 Ma weighted mean U-Pb age from the 13WW23 sample (Fig. 7B), which was taken from the same location as the J1352 fossil collection. The ~7-10 m.y. gap between the ca. 504 Ma zircon age and the ca. 497 Ma relative fossil age of the carbonate rocks could simply reflect uncertainty between all the ages, including those of the globally calibrated time scale (Fig. 14). Alternatively, the gap in ages could reflect transitions between volcanic eruptions and carbonate deposition, or that the zircon grains recovered from 13WW23 are of detrital origin and only constrain a maximum depositional age on the Egaksrak carbonate strata. In addition, the structural complexity, in both the southern and central belts, obscures many of the stratigraphic and relative age relationships between the carbonate and volcanic rocks. A somewhat cogenetic relationship between the carbonate and volcanic rocks, however, is supported by the prevalence of volcanic material observed in outcrops and thin sections of the carbonate rocks in the southern and central belts of the allochthon.

The upper age limit of the central belt is constrained only by the Furongian age of the faunas from the Egaksrak formation. Reiser et al. (1980), however, did map equivalents of the Romanzof formation in the interior parts of the central belt. Although we never traversed those locations, we did observe several sequences of volcaniclastic phyllite beds with minor chert, which could

correlate to the Romanzof formation in the southern belt. The presence of this formation implies that some of the central belt rocks can be assigned to the Upper Ordovician.

The rocks of the northern belt, assigned in this study to the Ekaluakat formation (Fig. 2), are the least constrained in terms of age, and correlation to the other belts of the allochthon is uncertain. The zircon U-Pb ages from a tuffaceous sandstone unit of the Ekaluakat formation, reported from sample 12JT35 of Johnson et al. (2016), have a nearly unimodal age distribution centered at ca. 500 Ma. This overlaps with the zircon U-Pb ages reported from the southern and central belts, and it implies that the volcanic and volcaniclastic rocks from all three belts formed at roughly the same time. The ca. 484 Ma K-Ar age reported by Reiser et al. (1980) also falls within the general ca. 512–452 Ma age range of rocks from the southern and central belts; however, the age is characterized by very low precision (±20 m.y.).

Several fossil localities, most of which include Ordovician and Silurian graptolite genera, have been reported from argillite and slate units in the northern belt (Reiser et al., 1980; Lane et al., 1995); however, most of these rocks are now considered part of the Cambrian–Ordovician Leffingwell formation or the Upper Ordovician-Lower Devonian(?) Clarence River Group (Johnson et al., 2016; Nelson et al., this volume; Strauss et al., this volume, Chapter 23). Despite these potential geochronological connections and proposed stratigraphic revisions, it remains possible that rocks of the northern belt do not correlate with the other two belts and therefore are not part of the Whale Mountain allochthon. Johnson et al. (2016) speculated that the ca. 500 Ma volcaniclastic strata had formed by recycling of Whale Mountain allochthon rocks from the southern and/or central belts and that they belonged to the younger Clarence River Group. This may be supported by the fact that the volcanic and volcaniclastic rocks in the northern belt are imbricated with Clarence River Group strata along several small-scale, north-directed thrust faults (Kelley et al., 1994; Lane et al., 1995), whereas the central and southern belts are abruptly separated from the other rocks in the NE Brooks Range by largescale thrust faults that cross the entire map area.

Paleogeographic Setting of the Whale Mountain Allochthon

Constraining the paleogeographic setting of the Whale Mountain allochthon is of first-order significance to reconstructing the early Paleozoic history of the circum-Arctic region. Previous investigators (e.g., Lane, 1991; Cecile et al., 1999; Lane et al., 2016) linked the volcanic rocks in the NE Brooks Range, herein treated separately as the Marsh Fork, Whale Mountain, and Ekaluakat units, to lower Cambrian–Upper Ordovician rift-related alkaline basalt and ultrapotassic flows that are exposed within off-shelf areas of the ancestral NW Laurentian margin, including the Selwyn Basin, Kechika trough, and elsewhere in the Canadian Cordillera (Hart, 1986; Goodfellow et al., 1995; Cecile et al., 1997; Pyle and Barnes, 2003). The lithostratigraphic, geochemical, and paleontological evidence presented in

this study reveals a more complex story of the Whale Mountain allochthon, making paleogeographic links between the allochthon and the Canadian Cordillera problematic. We argue that the Whale Mountain allochthon represents a diverse assortment of oceanic rocks originating outboard of the Laurentian margin that were assembled into an ancient accretionary wedge that formed in front of an Iapetus subduction zone.

Constraints from Lithofacies and Biofacies

The lithofacies and biofacies of the sedimentary rocks from the allochthon record a variety of depositional settings, and the mixed stratigraphic relationships with the mafic volcanic rocks resemble the chaotic architecture of an accretionary complex. In the southern belt, lithofacies from individual blocks or outcrops of the Egaksrak formation reflect deposition in periplatformal carbonate slope, shallow-marine oolitic shoal, and peritidal shelf environments. In many ways, the Egaksrak blocks resemble the Oman Exotics of the Hawasina Nappes in eastern Oman (Searle and Graham, 1982; Pillevuit et al., 1997), or the Calera Limestone units of the Franciscan Complex in northern California (Tarduno et al., 1985). Similar to these analogs, the interlayered architecture of Egaksrak carbonate units and the Marsh Fork volcanic rocks likely resulted from several processes, including finegrained pelagic settling of carbonate sediment on the basin floor, gravity sliding and mass transport of shallow-marine sediment, or repeated structural imbrication.

The faunal collections from the southern belt, including the early Cambrian fauna with Olenellus reported by Dutro et al. (1972) and the new collection from locality J1475, contain taxa that are common in deep-marine facies. Olenellus, while common in deeper-shelf and proximal off-shelf environments, was widely distributed across the facies belts that surrounded Laurentia (e.g., Palmer and Halley, 1979). The collection from locality J1475, however, unequivocally represents a deep-marine, off-platform fauna. Sclerites of the ceratopygid genus Aplotaspis make up more than 55% (30 of 54 specimens) of collection J1475. Ceratopygid trilobites are dominant, or at least major components, of deep-marine faunas in the upper Cambrian sections of several paleocontinents. The lower Furongian Proceratopyge rectispinata fauna described by Pratt (1992) from the Rabbitkettle Formation in northwestern Canada is a good Laurentian example, as is the Franconian 2 fauna in the Hillard Limestone of eastern Alaska from which Palmer (1968) described Yuepingia glabra.

Many other non-Laurentian occurrences of ceratopygidrich, deep-marine biofacies have been reported from the Furongian and uppermost strata of Miaolingian in Asia and Australia. *Aplotaspis* and *Proceratopyge* are key elements of lower-slope biofacies described from Siberia (Pegel, 2000). They also abound in deep-marine deposits of the Georgina Basin of northeastern Australia (Henderson, 1976) and played a major role in zonation of the thick, deep-marine succession of the Jiangnan slope belt that bordered the Yangtze Platform in China (Peng, 1992). The high percentage of agnostoid arthropods in J1475, which make up 28% (12 out of 54) of the specimens recovered, is greater than

that typically found in shallow-marine faunas but comparable to relative abundances of agnostoids reported for many collections that represent deeper-shelf to off-platform biofacies (e.g., Pratt, 1992; Westrop, 1995).

The Romanzof formation records hemipelagic sedimentation dominated by suspension rainout of fine-grained siliciclastic and biogenic detritus (Reiser et al., 1980; Moore, 1987; Mull and Anderson, 1991; Anderson et al., 1994; Nelson et al., this volume; Strauss et al., this volume, Chapter 23); furthermore, the lack of fine-grained pelagic carbonate deposits in the Romanzof formation most likely reflects deposition below the carbonate compensation depth. Fine-grained strata of the Romanzof formation are locally interbedded with lithic arenites and wackes that could represent trench-filling deposits, delivered by turbidity currents and sourced from an active volcanic margin (Strauss et al., this volume, Chapter 23).

The sedimentary rocks of the central and northern belts, although different in terms of their individual depositional settings, suggest sedimentation on or near a volcanic island. Similar to that described earlier from the southern belt, the Egaksrak formation of the central belt was most likely deposited in a combination of deep- and shallow-marine settings. The presence of interbedded volcanic matrix-supported lime rudstone, mudstone, and bioclastic grainstone at the J1352 locality reflects a combination of deep-marine suspension, sediment gravity, and turbidite sedimentation along a slope or steep-gradient setting. In contrast, the abundance of peloids, ooids, bioclasts, and rounded volcanic clasts (Fig. 4C) in some of the packstone and grainstone facies reflects some degree of reworking of shallow-marine carbonate sediment by wave action, as do the rounded clasts that compose the conglomeratic units that are interbedded with the basalt flows (Fig. 4G). The relative scarcity of agnostoids in faunal collections from sample localities J1352 and J1480 provides additional support for a shallow-water setting of the carbonate rocks in the central belt. Therefore, based upon the interstratification of shallow-water carbonates and alkaline basalt flows with oceanisland basalt (OIB) character, we interpret this belt to record deposition near an atoll or submerged volcanic island.

The Ekaluakat formation (Fig. 2) of the northern belt reflects deposition in a deep-marine basin, where the primary mode of deposition was pelagic and hemipelagic settling mixed with turbidity currents and possibly weak bottom currents. Notably, the sedimentary rocks of the Ekaluakat formation appear to lack abundant continental detritus. This is indicated by the near absence of detrital zircon grains older than 1 Ga from these units (Johnson et al., 2016) and by $\varepsilon_{Nd(r)}$ values >+4 in the fine-grained units (Nelson et al., this volume). Several tuffaceous and volcaniclastic units are also interbedded throughout the sedimentary section (Fig. 6D), further supporting deposition along or at the base of a submerged volcanic slope.

Constraints from Igneous and Zircon Geochemistry

The geochemical and petrological characteristics of Marsh Fork volcanic rocks in the southern belt closely resemble MORB. Their tholeiitic character (Fig. 8), unfractionated concentrations of Dy, Y, Yb, and Lu, and the gentle slopes on the normalized variation diagrams (Fig. 10) imply that the volcanic rocks were derived from a shallow (<80 km), garnet-free mantle source that was depleted in incompatible elements (e.g., Salters and Stracke, 2004; Kushiro, 2001). Shallow melting conditions and the eruption of tholeiitic basalt are most commonly found along midocean ridges, where the degree of partial melting is high and the flux of incompatible elements into the melt is diluted.

Although the southern belt samples show overall enrichment of most trace elements compared to the global average of MORB (Arevalo and McDonough, 2010), the trends on normalized variation diagrams are nearly parallel (Fig. 10). The enrichment was likely driven by postmelting crystallization of the magma. Some oceanic-island-arc suites have similar trace-element trends, but most of these suites also include negative Nb and Ta anomalies (e.g., Elliott, 2003). Furthermore, the >50 Ti/V ratios (Fig. 9A) are significantly higher than most island-arc suites (Shervais, 1982). Tholeitic basalt is also common in oceanic and continental flood basalt provinces; however, these suites are typically more enriched in the incompatible elements with respect to MORB-type lavas (e.g., Hooper and Hawkesworth, 1993).

The volcanic rocks from the central and northern belts have petrological and geochemical characteristics that resemble alkaline basalt. Alkaline magmas are produced in a variety of tectonic settings, but empirical models show that alkaline magmas are typically generated under deep, high-pressure conditions that suppress the amount of partial melting and concentrate incompatible elements into the melt (e.g., Yoder and Tilley, 1962; Green and Ringwood, 1967; Jaques and Green, 1980). A deep melting regime for the central and northern belt suites is supported by the relative depletions of Dy, Y, Yb, and Lu. These elements are typically withheld from the melt if the mantle source includes refractory garnet, which becomes stable at the expense of spinel below 85 km depth (Robinson and Wood, 1998). Deep melting conditions are further supported by the low oxygen fugacities inferred from the <50 Ti/V ratios (Shervais, 1982).

The enrichment of incompatible elements observed in the central and northern belt suites is also linked to melting of an enriched or fertile mantle source. There are several hypothesized types of fertile sources in the mantle (Hofmann, 2003), but melting of such sources typically requires a deep thermal anomaly or hotspot. Hotspot volcanism is commonly observed at intraplate oceanic-island settings or at off-axis seamounts, and the incompatible element trends of the central and northern belt suites follow the global OIB average (Sun and McDonough, 1989); however, similar trends have been observed from continental hotspots, including those found along the Cameroon line of western Africa (Fitton, 1987).

Isotopic compositions are particularly useful for determining mantle source geochemistry, because most isotopes do not fractionate during partial melting or crystallization processes. Although we did not measure any isotopes from our basalt

samples, the $\varepsilon_{Hf(t)}$ zircon values of +4 to +11 from the two samples, 15BJ06 and 13WW23 (Fig. 7), present several implications. Notably, the $\varepsilon_{Hf(r)}$ values are slightly displaced from the depleted mantle trajectory of Vervoort and Blichert-Toft (1999). This could imply that the source material from which the zircon crystallized was derived from (1) isotopically fertile mantle sources, (2) melts of Neoproterozoic crust, or (3) mixed depleted mantle melts and older (Paleoproterozoic?) crustal contaminants. Given the prevalence of mafic melts recorded in our geochemical data set and the absence of silicic melts, the volcanic rocks of the allochthon were not likely generated by crustal melting or assimilation. A cogenetic relationship between the melts that produced the volcanic rocks and those from which the zircon crystallized implies that the displaced $\epsilon_{Hf(t)}$ values, like the OIB geochemical signatures, reflect derivation from an isotopically fertile mantle source. Future studies that directly measure the isotopic compositions of the volcanic rocks will test this interpretation.

The segregation of MORB-type rocks in the southern belt from OIB-type rocks in the central and northern belts is a perplexing issue. Plausibly, the rocks from all three belts could have formed in different tectonic settings, or each belt could reflect temporal changes in melting conditions. Although OIB- and MORB-type lavas can be found in continental rift settings, MORB-type rocks are typically subordinate, and none of samples analyzed in the study exhibited the ultra-alkaline character observed in many rift provinces (e.g., Kampunzu and Mohr, 1991). The volcanic rocks of the Whale Mountain allochthon thus either formed by conventional oceanic melting mechanisms, mid-ocean-ridge decompression or intraplate hotspots, or they formed by renewed extension along a previously attenuated segment of continental crust, such as the continent-ocean transition at the distal reaches of a passive margin.

Interpretations that link the volcanic rocks in the NE Brooks Range to extensional events along NW Laurentia typically cite similarities with the alkaline volcanic rocks exposed in the Selwyn Basin (e.g., Lane et al., 2016). These include the Old Cabin Formation and Nibbery volcanic rocks, which are characterized by pillowed basalt flows that are interbedded with the off-shelf carbonates of the Rabbitkettle Formation (Hart, 1986; Cecile, 2000; Goodfellow et al., 1995). The base of Old Cabin Formation is constrained by a 499 Ma zircon U-Pb age (MacNaughton et al., 2016), which overlaps with the zircon ages reported in this study. Goodfellow et al. (1995), however, showed distinct geochemical differences between the Whale Mountain volcanic rocks and the volcanic rocks of the Selwyn Basin, suggesting that the Selwyn Basin volcanic rocks formed by partial melting of lithospheric mantle, whereas the Whale Mountain volcanic rocks formed by partial melting of enriched portions of the asthenosphere. In addition, the MORB-like basalt flows and imbricated chert units in the southern belt of the allochthon, which were not examined in the Goodfellow et al. (1995) geochemical study, are unlike anything exposed in the Selwyn Basin or the Canadian Cordillera.

In many ways, the Whale Mountains allochthon resembles the Franciscan Complex in northern California, which includes a wide array of both tholeiitic and alkaline volcanic rocks mixed with both deep-marine chert and shallow-marine limestone (e.g., Shervais and Kimbrough, 1987; Tarduno et al., 1985; MacPherson et al., 1990). The Hawasina Nappes in eastern Oman are another good analog, where chaotic mélanges of intercalated alkaline volcanic and shallow-marine carbonate rocks, the Oman Exotics, are imbricated with deep-marine sedimentary and subordinate tholeiitic volcanic rocks, all of which were thrusted onto passive-margin sequences of the Arabian Platform during the closure of the Tethys Ocean (e.g., Béchennec et al., 1990; Pillevuit et al., 1997).

Constraints from Paleobiogeography

The most unequivocal tie to Laurentia provided by the faunas from the Egaksrak formation is the Olenellus reported by Dutro et al. (1972) from their Marsh Fork locality. This uniquely Laurentian genus was widely distributed across the facies belts that surrounded Laurentia in the early Cambrian (e.g., Palmer and Halley, 1979), but it is particularly common in intermediateand deep-marine facies that accumulated in open-shelf and offshelf environments. If the cranidium from locality J1475 identified here as *Stenopilus*? sp. does represent that genus, which is uncertain (see Appendix 1), it reinforces the evidence of proximity to Laurentia provided for the southern belt by Olenellus. Stenopilus is one of several plethopeltid genera closely associated with microbial reefs of the Laurentian platform (Ludvigsen and Westrop, 1983; Taylor et al., 2009), but it also occurs in deepmarine, toe-of-slope deposits sourced by downslope transport of sediment from reefs at the platform margin and upper slope (Ludvigsen et al., 1989). Like Olenellus, Stenopilus is uniquely Laurentian, and it requires at least proximity to that paleocontinent. However, having been reported from both platform and off-platform deposits, neither of these genera resolves whether the volcanic rocks of the southern belt were extruded on the Laurentian platform or were part of an oceanic volcanic succession outboard of the Laurentian margin.

Dutro et al. (1972) based their interpretation of the fauna at their Leffingwell Fork locality as one of North American (i.e., Laurentian) aspect on assignment of a single, fragmentary cranidium to the idahoiid genus Saratogia. This was a reasonable conclusion, given the prevalence of Saratogia and other idahoiids in early Sunwaptan faunas described previously from Montana and Wyoming (Grant, 1965), Texas (Longacre, 1970), and Oklahoma (Stitt, 1971). It was also reported in later studies of coeval faunas in Alberta (Westrop, 1986) and the Appalachians (Ludvigsen and Westrop, 1983; Taylor et al., 2009). However, the large collection (J1480) recovered in 2014 from the Leffingwell Fork locality reveals that it is not a typical Saratogia/Idahoia zone fauna. As explained in detail in Appendix 1, J1480 is dominated by two new idahoid species that cannot be assigned to any established genus. Saratogia is not represented, nor are other genera that characterize faunas of this age in various facies across Laurentia, such as Drumaspis, Wilbernia, and Ptychaspis.

Wilbernia is particularly widespread, occurring not only in most idahoiid-rich early Sunwaptan platform faunas, but even in coeval slope deposits in the Rabbitkettle Formation in NW Canada (Westrop, 1995). Drumaspis is similarly widespread in both shallow- and deep-marine faunas, the latter including the "Franconian 2" fauna described by Palmer (1968) from the Hillard Limestone, the off-platform equivalent of the Jones Ridge Formation in east-central Alaska. Although the dominance by idahoiids does suggest proximity to Laurentia, the absence of all characteristic and widespread Saratogia/Idahoia zone genera is difficult to reconcile with origination on or even directly adjacent to the Laurentian platform. The only specimens in J1480 that might represent a Laurentian genus are three cranidia assigned with considerable uncertainty to Plethopeltis (Figs. 12T-12W). These cranidia to some extent resemble Plethopeltis saratogensis, a species associated with Saratogia in the Appalachians (Ludvigsen and Westrop, 1983; Taylor et al., 2009), but they differ in some critical features (Appendix 1). Given these differences, the poor preservation, and lack of an associated pygidium or librigena, the assignment is quite tentative, and the link to Laurentia is equally tenuous.

The strongest evidence that the Egaksrak formation in the central belt did not originate on the Laurentian platform is provided by collection J1352, which consists of 127 specimens recovered from strata interstratified with pillow basalt and volcaniclastic rocks. Except for one cranidium, which probably represents Cheilocephalus, the fauna is remarkably unfamiliar. The species are distinct and specialized individually and collectively display a wide range of morphologies. Such differentiated faunas in the Laurentian platform succession characterize the middle to upper parts of the Cambrian stages, and the constituent genera and species are easily recognized as Laurentian taxa and diagnostic of their respective zones. The diverse faunas of the Crepicephalus, Elvinia, and Saukia zones at the tops of the Marjuman, Steptoean, and Sunwaptan Stages, respectively, exemplify this, and at least a few of the endemic genera that characterize those zones are found consistently in coeval deep-marine deposits that accumulated along the Laurentian margin (Raymond, 1924; Rasetti, 1944; Palmer, 1968; Ludvigsen et al., 1989; Pratt, 1992; Westrop, 1995). None of the five to six genera in J1352 could be assigned to any established genus from Laurentia, or any other paleocontinent. For this reason, the paleogeographic model we favor for the rocks of the central belt is extrusion in an oceanic setting close enough to Laurentia for very limited interchange with the shallow-marine faunas of that paleocontinent, and hence the idahoiids and possible Plethopeltis in J1480 and Cheilocephalus in J1352, but sufficiently removed to allow for evolution of unique, endemic trilobite faunas in the shallow environments around the volcanic islands.

The data presented in this study do not directly address whether the Whale Mountain allochthon formed outboard NW or NE Laurentia. A peri-Laurentian origin for the allochthon, as recognized by the faunal collections from the Egaksrak formation, aligns with recent models that restore portions of the

Arctic Alaska terrane to NE Laurentia in the early Paleozoic (e.g., Strauss et al., 2013, 2017, this volume, Chapter 23; Johnson et al., 2016). In the context of Mesozoic terrane boundaries, earlier studies grouped the pre-Mississippian rocks exposed in the NE Brooks Range and the Doonerak region of the central Brooks Range into the North Slope subterrane (e.g., Jones et al. 1987; Moore et al., 1994). The recent models of Strauss et al. (2017), however, severed the early Paleozoic ties between the Doonerak region and the North Slope, suggesting that the Ordovician-Silurian volcanic assemblages at Doonerak formed in response to subduction of Iapetus lithosphere outboard NE Laurentia, whereas the rocks of the North Slope had formed as a lateral continuation of the deep-marine, Franklinian Basin at northern Ellesmere Island in Arctic Canada (Johnson et al., 2016; Nelson et al., this volume; Strauss et al., this volume, Chapter 23). This restoration calls for an ancient oceanic basin or marginal seaway that separated the North Slope from the Doonerak arc in the early Paleozoic. We contend that the Whale Mountain allochthon is a relic of this basin, and it now marks the early Paleozoic suture between the North Slope and the Doonerak region.

The exact paleogeographic configuration of the basin remains unclear because it is not possible, with the data presented in this study, to determine whether the rocks of the Whale Mountain allochthon formed in a true oceanic basin or in some type of marginal seaway that separated the Laurentian margin from outboard terranes. The faunal collections from the Egaksrak formation, particularly those of J1352, suggests that at least some portion of the allochthon formed in an open-ocean setting, allowing for faunal communities of the Egaksrak formation to evolve in isolation. The assembly and emplacement of the allochthon are also unclear. The allochthon's structural position above Upper Ordovician—Lower Devonian(?) strata of the Clarence River Group suggests that emplacement occurred in post—Early Devonian time (Johnson et al., 2016), but future work is needed to reconstruct the paleogeographic origins of each belt.

CONCLUSIONS

The general implications of this work reveal that the pre-Mississippian rocks of the NE Brooks Range cannot be assigned to a coherent stratigraphic architecture. The fault-bounded rocks of the Whale Mountain allochthon record a complex geological history, dating from Series 2 of the Cambrian (ca. 512 Ma) to the Late Ordovician (ca. 452 Ma). Field observations and igneous geochemistry show that the assorted igneous and sedimentary rocks formed in diverse depositional and tectonic settings, ranging from basin floor settings founded on MORB-type lavas to shallow platform settings that capped isolated volcanic islands. The new trilobite faunal collections from the Egaksrak formation greatly expand the biostratigraphic record of the NE Brooks Range, with important implications for reconstructing the paleogeography of northern Laurentia. A few of the identified species have loose affinities to Laurentia, but all three collections are missing

many of the diagnostic Laurentian platform species that are found throughout Upper Cambrian carbonate units from western to eastern North America. One of the fossil locations (J1352) yielded a collection of species that do not have a recognized affinity with any of the major late Cambrian paleocontinents.

We conclude that the rocks of the Whale Mountain allochthon did not form on the stable platforms that surrounded Laurentian in the late Cambrian, but instead formed in a peri-Laurentian setting, perhaps in the open waters of the Iapetus Ocean. The allochthon was later assembled when disparate rock assemblages were episodically scraped from a subducting oceanic plate into an ancient accretionary wedge and collectively emplaced onto the Laurentian margin at the time of basin closure.

APPENDIX 1: SYSTEMATIC PALEONTOLOGY

Illustrated specimens are reposited in the invertebrate paleontology collections at the Carnegie Museum of Natural History (prefix CM) in Pittsburgh, Pennsylvania, USA.

FAMILY AGNOSTIDAE M'COY, 1849 Genus *Micragnostus* Howell, 1935

Opinions vary widely regarding the relationships of several late Cambrian agnostoid genera, among them *Homagnostus*, *Micragnostus*, *Oncagnostus*, and *Trilobagnostus*. Recent discussions of the problem can be found in Choi et al. (2004) and Westrop and Eoff (2012). The approach taken by Choi et al. (2004) is adopted here, with the assignment of species with relatively short and parallel-sided glabellae and pygidial axes, and weakly developed or absent median preglabellar furrows to the genus *Micragnostus*.

Micragnostus sp.

Illustrations: Figures 12DD-12GG.

Remarks: The agnostoids in collection J1480, originally identified by Dutro et al. (1972) as *Geragnostus* sp., resemble in all respects the specimens illustrated by Westrop (1995, his plate and figs. 14–16) for *Micragnostus chiushuensis* (Kobayashi). However, the deformed nature of the specimens from the Egaksrak formation renders detailed comparison difficult and precludes certain assignment to that species. Accordingly, they are left in open nomenclature as *Micragnostus* sp. The reassignment from *Geragnostus* does not reflect a disagreement with the initial identification in Dutro et al. (1972); it results from a widely accepted revision of that genus by Fortey (1980), who restricted it to species possessing a complex F3 glabellar furrow divided into three segments, with the glabellar node located barely behind the central segment. Species like the one in J1480, which display an undivided F3 and more posteriorly placed glabellar node, now fall within *Micragnostus*.

Genus *Pseudagnostus* Jaekel, 1909 *Pseudagnostus josepha*? (Fig. 11DD)

Remarks: The morphology of the one, small pygidium in collection J1475 identified as *P. josepha*? falls within the broad concept used for *P. josepha* by Peng and Robison (2000). (See Westrop and Eoff [2012] for an alternate view of the range of variation that should be encompassed by this and other agnostoid species.) The Alaska pygidium is nearly identical to one of the small pygidia illustrated by Peng and Robison (2000, their fig. 10–5), differing only in displaying a slightly narrower border furrow and more firmly impressed axial furrow along the posterior half of the posteroaxis. Westrop (1995) and Chatterton and Gibb (2016) reported similar species that they left

in open nomenclature as *P.* cf. *P. josepha* from the Rabbitkettle Formation in the Northwest Territories and southeastern British Columbia, respectively.

Pseudagnostus aff. P. parvus Shergold, 1980 (Figs. 11Y-11AA)

Remarks: This species in collection J1475 resembles *P. parvus* in its long, parabolic cephalon with a long and relatively narrow glabella, anteriorly placed glabellar node just behind a nearly obsolete F3, fairly narrow borders, and broad, deep border furrows. It differs in displaying a more transverse (less rounded) anterior margin, and a broader and less pointed anterior glabellar lobe.

Genus *Neoagnostus* Kobayashi, 1955 *Neoagnostus*? sp. (Figs. 11BB–11CC)

Remarks: This single, fragmentary pygidium in collection J1475 resembles *N. canadensis* (Billings) in possessing well impressed but only weakly divergent axial furrows along the anterior half of the posteroaxis, and an exceptionally broad border furrow that is widest near the posterolateral corners. It resembles pygidia illustrated for this species by Shergold (1977, his plate 16 and fig. 10) and Ludvigsen et al. (1989, his plate 4 and fig. 7) in these respects, but it differs in the shallowing of the axial furrows along the posterior half of the posteroaxis and resultant lack of elevation of the back of the axis above the border furrow.

Agnostoid gen. sp. undetermined (Figs. 13DD-13EE)

Remarks: This one cephalon in collection J1352 resembles a number of Furongian species in genera such as *Homagnostus*, *Micragnostus*, and *Oncagnostus* in its forwardly placed glabellar node, short and somewhat inflated posteroglabella, relatively small basal lobes, and partial median preglabellar furrow. However, its small size and lack of an associated pygidium preclude certain assignment even to genus.

Class TRILOBITA Family IDAHOIIDAE Lochman, 1956

Remarks: The dominant trilobites in J1480 are confidently assigned to the Idahoiidae based on their anteriorly truncate, subtrapezoidal glabellae, large, band-like palpebral lobes, faintly impressed palpebral furrows, prominent dorsally and ventrally directed occipital spines, and broad preglabellar and librigenal fields traversed by genal cecae. Two distinct idahoiid species are represented in the collection. The cephalon for each species could be reconstructed owing to a contrast in depth of border furrows and slope of genal/preglabellar fields, which allowed recognition of the corresponding librigena for each cranidium. Unfortunately, neither of the two pygidia displays any trait to link it with the appropriate cephalon, and they are treated separately below as Idahoiid pygidium 1 and 2.

Ludvigsen and Westrop (1983) significantly revised the Idahoiidae in a monograph describing a fauna from New York that included Saratogia calcifera (Walcott), the type species of Saratogia. Among the changes was reduction of Idahoia to a subgenus of Saratogia, with separation of the subgenera based on contrasting pygidial morphologies. A long axis extending to the posterior margin, and a narrow, convex border characterize the pygidium of Saratogia (Saratogia), while species of Saratogia (Idahoia) have pygidial axes that terminate well in front of the margin at the inner edge of a broad, gently concave border. Neither pygidium in collection J1480 displays the requisite features to justify assignment to either of these subgenera, nor to any other idahoiid genus such Minkella, Meeria, and Psalaspis. A single cranidium, here referred to as Idahoiid? genus and species indeterminate, displays some of the characteristic features of Minkella, but it differs in too many respects to allow confident assignment to that genus.

Idahoiid new genus, new species 1 (Figs. 12A-12D)

Remarks: Although the basic form of the cranidium and librigena of this species is quite similar to that of *Saratogia*, it is set apart by the weak impression of its axial, border, occipital, and lateral glabellar furrows, even where exfoliated. The gentle and even slope of the preglabellar field and broad, only moderately impressed anterior border furrow are also distinctive.

Idahoiid new genus, new species 2 (Figs. 12E-12J)

Remarks: This species differs from the other idahoiid species in J1480 in its more deeply incised furrows, especially the anterior, lateral, and posterior border furrows. Other differences include a steeply downsloping preglabellar field, slightly upturned anterior border, and S1 furrows that bifurcate distally and terminate well short of the axial furrow. The palpebral lobes are also elevated above the level of the narrow interocular fixigenae. It shares many of these features with some species of *Saratogia* (Idahoia), such as *Saratogia* (I.) fria Lochman and Hu (1959). However, as noted above, neither of the associated idahoiid pygidia in J1480 is consistent with assignment to that genus.

Idahoiid pygidium 1 (Figs. 12R-12S)

Remarks: A strongly convex axis comprising three rings and a terminal piece is elevated well above abaxially downsloping pleural fields marked by three pairs of pleurae. The axis ends well forward of the posterior margin at the inner edge of a fairly wide border, as is typical of *Saratogia* (*Idahoia*) pygidia. However, the border is flat to slightly dorsally convex, as opposed to strongly concave in that subgenus, and it makes up significantly less of the sagittal length of the pygidium. The border also differs in being interrupted by a postaxial ridge and being traversed by the very narrow (exsagittal) posterior bands of the two anteriormost pleurae, for which intersection with the margin is marked by minute, inconspicuous terminal spines.

Idahoiid pygidium 2 (Figs. 12M-12Q)

Remarks: The axis, consisting of four axial rings and a terminal piece, is more parallel-sided and broader (transverse) at the posterior end than that of pygidium 1. The four pairs of pleurae display anterior and posterior bands of equal width (exsagittal) and pleural furrows that are relatively narrow and deeply incised. The pleural bands and furrows terminate at the inner margin of a gently convex border that is narrower (exsagittal) than that of pygidium 1, but much wider and less convex than that of *Saratogia* (*Saratogia*). The border ends adaxially at the sides of a broad postaxial ridge.

Idahoiid? genus and species indeterminate (Figs. 12K-12L)

Remarks: The small, thorn-like occipital spine and narrow anterior border on this single cranidium in J1480 resemble those of *Minkella*, but the palpebral lobes are longer than is characteristic of that genus, and the glabella is shorter relative to its width than that of any idahoiid. However, given the deformed condition of most sclerites in this collection, it is possible that the cranidium has experienced some anterior-posterior compression. Consequently, its assignment to the Idahoiidae is uncertain.

Genus *Plethopeltis* Ulrich in Bridge, 1931 *Plethopeltis?* sp. (Figs. 12T–12W)

Remarks: The cranidia identified as *Plethopeltis*? sp. resemble in most respects those of *Plethopeltis saratogensis*, a species associated with *Saratogia* in the lower Sunwaptan of New York (Ludvigsen and Westrop, 1983). However, the occipital ring preserved on the most complete cranidium (Figs. 12T–12U) does not expand posteriorly axially to produce a blunt occipital spine, as is characteristic of *P. saratogensis*. Instead, it displays a transverse posterior margin and remains fairly nar-

row (sagittal) across the axis. No species of *Plethopeltis* displays such an occipital ring. Given the atypical form of the occipital ring, and the absence of either a librigena or pygidium to reinforce or refute assignment to *Plethopeltis*, the generic assignment is questionable.

Genus Stenopilus, Clark, 1924 Stenopilus? sp. (Figs. 11N-11P)

Remarks: A single, effaced (smooth) cranidium in collection J1475 is assigned with reservation to the genus *Stenopilus*, owing to its strong sagittal and transverse convexity, relatively short (exsagittal) posterior areas, and strongly convex, overhung posterior margin. Certain assignment to that genus is not possible, however, because tightly adhering matrix made it impossible to expose the anterior and lateral margins to confirm the presence of a strong anterior arch, and small eyes on the steeply sloping sides of the cranidium. These features set *Stenopilus* apart from other effaced genera.

Family CERATOPYGIDAE Linnarsson, 1869 Genus *Aplotaspis* Henderson, 1976

An anteriorly tapering glabella, narrow (exsagittal) posterolateral extensions, and a concave pygidial border identify the ceratopygid that dominates collection J1475 as a species of either Aplotaspis Henderson (1976) or Yuepingia Lu (1956). The eyes are larger than is typical of Aplotaspis, more closely resembling those of Yuepingia, but most cephalic and pygidial characteristics are more compatible with assignment to the former genus. Yuepingia niobiformis displays a concave pygidial border, but it is much narrower than the strongly convex pleural fields, unlike the very broad border in Aplotaspis, which equals or exceeds the width of more restricted, flatly convex pleural fields. All other species of Yuepingia for which pygidia have been described have either a narrow, flat to gently convex border, or no border at all, with pleural furrows and the pygidial axis extending almost to the margin. The pygidial axis of *Aplotaspis* ends at the inner edge of the wide, concave border, and it is followed posteriorly by a faint, tapering postaxial ridge that extends to the margin. All but the most anterior pair of faintly impressed pleurae also terminate at or just beyond the inner edge of the border. A similarly broad, concave lateral border, equal in width to the genal field on the librigena of *Aplotaspis* n. sp. (Fig. 11G), also supports assignment to that genus, resembling that of the type species, A. erugata (Whitehouse), and contrasting with the relatively narrow, flat to convex borders that characterize species of Yuepingia.

A rigorous, parsimony-based reevaluation of these genera, and closely related taxa such as Charchagia and Pseudoyuepingia, is badly needed but falls beyond the scope of the present study. At present, such an analysis would be severely hampered by the large number of species for which the pygidium and/or librigena remain unknown, and little if any information on ontogenetic variation is available. An example of such limitations can be found in Henderson (1976), wherein much smaller palpebral lobes were included among the primary characteristics that set *Aplotaspis* apart from *Yuepingia*. The deficiency in the comparison is that the single cranidium of Yuepingia illustrated (Henderson, 1976, his plate 48 and fig. 12), with palpebral lobes conspicuously larger than those shown for Aplotaspis, is a small sclerite only half the size of the figured Aplotaspis cranidia. As relative size of the palpebral lobes usually decreases through ontogeny (compare Figs. 11D and 11A herein), the size difference of the illustrated specimens exaggerates the contrast in the size of this feature between the genera. Future work may ultimately confirm that species of Yuepingia consistently display larger eyes than those of Aplotaspis, but that hypothesis is yet to be tested through quantitative comparison of collections large enough to account for ontogenetic variation.

Bao and Jago (2000) placed *Aplotaspis* in synonymy with *Charchaqia*, arguing that the width of the pygidial border is too variable within *Charchaqia* to justify placement of species with a longer border in a separate genus, i.e., *Aplotaspis*. As evidence, they noted variability

in the width of the border on pygidia figured by Henderson (1976) for the type species of Aplotaspis (A. erugata), and on pygidia of Charchaqia halli that they illustrated from Tasmania. Unfortunately, two of the specimens of C. halli (Bao and Jago, 2000, their plate 2 and figs. 1 and 2) are internal molds on which the imprint of the pygidial doublure gives the false impression of a relatively broad, concave border. The two rubber casts made from external molds (Bao and Jago, 2000, their plate 2 and figs. 1 and 2) show that the convex pleural fields actually extend nearly to the margin, terminating at the inner edge of a very narrow, convex border. A quantitative comparison of border length/ pygidial length ratios (discussed below) between the two genera, utilizing figured specimens of several species in both, does not support the claim of intergrading variation, and their synonymy is rejected. Aplotaspis is retained as a separate genus, and a broad, dorsally concave border on the librigena and the pygidium remains one of the primary features that distinguish it from Charchagia, Yuepingia, and Pseudoyeupingia.

The pygidial border length used for comparison of these genera was obtained by measuring the distance along the axis from the posterior margin to the point on the axis in line with the inner edge of the border. That axial border length was divided by the axial length of the pygidium (excluding the articulating half ring) to obtain a border/length ratio that expresses the percentage of the pygidial length constituted by the border. Although border width does vary somewhat in Aplotaspis erugata, measurements from the images of four pygidia illustrated by Henderson (1976) reveal that the concave border makes up at least a third of the axial length of the pygidium, and in some specimens accounts for nearly half. The ratios obtained for the four pygidia of Aplotaspis erugata ranged from 0.34 to 0.45. The border constitutes just over half (border/length ratio = 0.51) of the axial length of the pygidium figured for Aplotaspis mucrora (Henderson, 1976, his plate 48 and fig. 14). In contrast, species of Charchaquia display short (sagittal), flat to upwardly convex borders that constitute no more, and usually considerably less, than one fifth of the axial pygidial length. Pygidia illustrated by Peng (1992) for the type species of Charchaqia, Charchaqia norini (his fig. 53L), and for Charchaqia glabrescens (his fig. 55F) yielded border/length ratios of 0.19 and 0.125, respectively. The border/length ratio determined for Charchagia lata Troedsson (Chien, 1961, his plate 5 and fig. 2) is 0.13. As previously noted, the concavity along the margin of the internal molds of C. halli illustrated by Bao and Jago (2000, their plate 2 and figs. 1 and 2) is the imprint of the pygidial doublure. The true border, visible on their figure 3, is an extremely narrow, convex rim that yields a border/length ratio less than 0.05.

Aplotaspis new species (Figs. 11A-11M)

Aplotaspis n. sp. is most similar to A. erugata in displaying an ellipsoidal pygidium that is much wider (transverse) than long, with a transverse margin behind the axis, as opposed to the subcircular pygidia of A. mucrora and A. caelata, and subtriangular pygidium of A. ex. gr. erugata Varlamov et al. (2006). It also resembles the genotype in its very narrow (exsagittal), strap-like posterolateral projections, unequally divided by a well-impressed border furrow into wider posterior borders and exceptionally narrow posterior fixigenae. It differs from A. erugata in having more gently concave cephalic and pygidial borders, the inner boundaries of which are marked by faint ridges rather than distinct furrows, and significantly larger palpebral lobes. In both species, the back of the palpebral lobe sits approximately in line with the glabellar node. The palpebral lobes in A. erugata and A. mucrora extend forward only approximately halfway to the front of the glabella from the glabellar node. Those of Aplotaspis n. sp. extend more than two thirds of the way, resembling species of Yuepingia, such as Y. niobiformis Lu and Y. glabra Palmer, in this regard. It is distinguished from those species by the greater length of the frontal area, broad and concave lateral and pygidial borders, and much wider (transverse) and

less convex pygidium. The only species of *Yuepingia* that displays a frontal area as long (sagittal), and librigena as broad (transverse) as *Aplotaspis* n. sp. is *Yuepingia brevica* Lu and Zhu (1980), for which only two poorly preserved cranidia and one librigena are illustrated. The cranidia display more parallel-sided glabellae than *Aplotaspis* n. sp., and the librigena is unequally divided by a shallow border furrow into a broad genal field and much narrower, dorsally convex border. With no associated pygidium to assist in generic assignment, it is uncertain whether *Y. brevica* is properly placed in *Yuepingia*. Although the material available for *Aplotaspis* n. sp. is adequate to confirm that it is a new species, the specimens are too few and fragmentary to allow complete description and naming of the new taxon.

FAMILY CHEILOCEPHALIDAE SHAW, 1956 Genus *Cheilocephalus* Berkey, 1898

Cheilocephalus? sp. (Figs. 13A-13D)

Remarks: A single, small cranidium in collection J1352 displays most of the diagnostic features of this genus. Small, forwardly placed palpebral lobes are centered opposite weakly impressed S2 furrows, creating large triangular posterior areas. Short (exsagittal) and narrow, dorsally concave anterior fixigenae lie between faint eye ridges and a very narrow, convex, anterior border. It also displays (Figs. 13C-13D) the characteristic sharp downward flexure and slight inflation of the posterior border directly behind the palpebral lobe, referred to by Palmer (1965) as a "shoulder" and analyzed in greater detail by Westrop et al. (2008). This species is left in open nomenclature, rather than being assigned to Cheilocephalus without reservation, only because there is no associated pygidium or hypostome to fortify such assignment. Of the Laurentian species that display similar granular sculpture, Cheilocephalus? sp. most closely resembles Cheilocephalus brachyops Palmer (1965), especially the small cranidium (Palmer, 1965, his plate 1 and fig. 14) illustrated from Shingle Pass, Nevada. Like that small (axial length ~2 mm) cranidium of C. brachyops, the small (3.2-mm-long) cranidium in J1352 displays a short, nearly quadrate glabella and extremely short frontal area. The J1352 cranidium differs in having less strongly divergent posterior branches of the facial suture, narrower (transverse) and more steeply downsloping posterior areas, more distinct and slit-like S2 furrows, and a less transverse anterior margin that is curved backward strongly in front of the eye ridges. The weakly divergent posterior facial sutures set the Alaska species apart from all other species of Cheilocephalus. However, no comparably small cranidia have been illustrated for Cheilocephalus granulosus Palmer, nor for Cheilocephalus buttsi Resser, a species from the Ore Hill limestone in Pennsylvania (Wilson, 1951), in which unusually narrow (transverse) anterior fixigenae resemble those of Cheilocephalus? sp.

Family UNCERTAIN

The collections from the Egaksrak formation include at least 10 additional species for which no suitable genus could be found. These are left in open nomenclature as genus species indeterminate (gen. sp. indet.) with a number and letter designation, where the number is the last two digits of the collection number. Eight of these species are represented by only one or two fragmentary sclerites.

Genus species indeterminate 52A (Figs. 13E–13H)

Remarks: This species, represented by a single cranidium and fragmentary librigena, resembles some Steptoean (Paibian) genera such as *Drabia* and *Sulcocephalus*. It resembles *Drabia* in the basic form of the cephalon, and *Sulcocephalus* in its more rounded glabella and deep S1 furrow isolated from the axial furrow. Neither of those genera, however, has the elevated occipital ring (LO), discontinuous occipital furrow (SO), and relatively broad and heavily terraced cephalic border displayed by gen. sp. indet. 52A.

Genus species indeterminate 52B (Figs. 13I-13N)

Remarks: This species resembles *Croixana* Nelson, 1951, in its subtrapezoidal, anteriorly truncated glabella and inflated frontal area, with the anterior border furrow expressed only at the anterolateral corners. However, it lacks the characteristic pits created by deepening of the axial furrow at the anterior corners of the glabella. It also differs from all known species of *Croixana* (see Westrop, 1986) in its exceptionally long palpebral lobes (>2/3 the length of the glabella), centered well behind instead of opposite the 2S furrows, and wide interocular fixigenae, which are nearly half the width of the glabella at its midlength. The anterior border furrow also differs in trending laterally and slightly anteriorly inward from margin, rather than being directed posterolaterally toward the anterior corners of the glabella as in *Croixana*.

Genus species indeterminate 52C (Figs. 13O-13V)

Remarks: Distinctive features of this common species in J1352 include a gently anteriorly tapering glabella with sigmoid S1 furrows that bifurcate distally without reaching the deep and narrow axial furrows; a moderately convex cephalic border of constant width separated from slightly inflated genal fields by a narrow well-impressed furrow, and from the glabella by a narrow, slightly depressed preglabellar field; an inflated occipital ring with an ellipsoidal shape created by strong curvature of its posterior margin; an SO that is shallow and bowed forward over the axis, deepening and broadening behind L1; and widely spaced, coarse granules covering the glabella and genal fields. Fine, closely spaced granules cover the librigenal spine and pleural bands and axial rings of the pygidium. A broad border furrow that narrows behind the axis separates moderately convex pleural fields crossed by narrow, well-impressed pleural furrows from a very narrow convex border. The posterior margin rises adaxially to create a shallow notch behind the axis.

Genus species indeterminate 52D (Figs. 13W-13Y)

Remarks: The two cranidia in J1352 that represent this species display many of the features that characterize gen. sp. indet. 52C, but they differ in being wider than long and more strongly convex (sagittal and transverse), and having a much narrower anterior border that is more tapered and more strongly directed abaxially.

Genus species indeterminate 52E (Figs. 13Z-13AA)

Remarks: No associated cranidium, or established Furongian genus, was found to be compatible with the broad, flat to gently concave genal field, dense granular sculpture, long and inwardly curved anterior facial suture, and prominently terraced border of this single librigena in J1352.

Genus species indeterminate 52F (Figs. 13BB-13CC)

Remarks: The dense texture of coarse granules and broad, convex border of this single librigena in J1352 confirm that it has no corresponding cranidium in the collection. No genus was found with librigenae displaying those features and a minute, cylindrical, laterally directed librigenal spine.

Genus species indeterminate 75A (Figs. 11Q-11T)

Remarks: Two fragmentary cranidia in collection J1475 represent this granulose species, which has an inflated anterior border that tapers rapidly abaxially behind a strongly curved anterior margin, and in front of a transverse border furrow that shallows over the axis in front of a narrow, sunken preglabellar field.

Genus species indeterminate 75B (Figs. 11U–11V)

Remarks: A single librigena and fragmentary cranidium in collection J1475 represent this species. They are readily matched by a long, strongly divergent anterior branch of the facial suture, a relatively

short (exsagittal) and elevated palpebral lobe, and scattered coarse granules on the fixigenae and steeply downsloping genal field, which terminates distally at the inner edge of a broad (transverse) gently convex lateral border.

Genus species indeterminate 75C (Figs. 11W-11X)

Remarks: This single, fragmentary pygidium in collection J1475 displays a broad, strongly convex, parallel-sided axis elevated above flat to slightly concave pleural fields with prominent depressed areas near the posterior margin in line with the sides of the axis.

Genus species indeterminate 80A (Figs. 12X-12Z)

Remarks: This species is represented by several poorly preserved cranidia in collection J1480 that resemble those of *Plethopeltis*? sp. in basic form, but they display a narrow (sagittal), laterally tapering anterior border and a prominent eye ridge.

Genus species indeterminate 80B (Figs. 12AA-12CC)

Remarks: This single, fragmentary, triangular pygidium in collection J1480 displays a posteriorly tapering, flat-topped axis with narrow (sagittal) axial rings separated by deep ring furrows, narrow and similarly incised pleural fields, and a steeply downsloping, gently convex, and terraced border that narrows adaxially and might disappear entirely at the axis where the deeply notched posterior margin reaches its highest point.

ACKNOWLEDGMENTS

Johnson and Toro thank West Virginia University's Faculty Senate Grant and the Circum-Arctic Lithosphere Evolution (CALE) project for providing financial support. Strauss was supported by a National Science Foundation (NSF) Graduate Research Fellowship and a grant from the NSF Tectonics Division (EAR-1624131). Financial support for study of the faunas was provided through a NSF Sedimentary Geology and Paleobiology grant (award 1325333) to Taylor, who also acknowledges invaluable assistance from fellow paleontologists J.R. Laurie and S.R. Westrop in evaluating the taxonomic and paleogeographic affinities of the trilobites and agnostoid arthropods of the Egaksrak formation. Indiana University of Pennsylvania students W.T. Kamerer and J.D. King assisted in the analysis of the faunas through senior research projects on the agnostoids and trilobites, respectively. The Geological Society of America Graduate Student Research Fellowships also supplied additional funding to Johnson, Strauss, and Ward. Field work in 2013 was conducted through the Circum-Arctic Structural Events (CASE) 13 expedition to northern Yukon, which was graciously supported by the Bundesanstalt für Geowissenschaften und Rohstoffe (BGR) and Yukon Geological Survey. We thank Karsten Piepjohn of BGR for funding the CASE 13 expedition, and Blaze Budd, Patrick Frier, and Lyle Nelson for assistance in the field. Kirk Sweetsir from Yukon Air Service and the staff at Wright Air Service provided critical access to our remote field area. Permission to work in the Arctic National Wildlife Refuge was granted by Alfredo Soto at the U.S. Fish and Wildlife Service. Many of the ideas presented herein were conceived during spirited discussions with Tom Moore, Gil Mull, Francis Macdonald, Marwan Wartes, Tyrone Rooney, Elizabeth Miller, Eric Gottlieb, and Tim O'Brien. Finally, we are grateful to Carl Hoiland and Brian Pratt, who provided thoughtful reviews that drastically improved the manuscript, and we appreciate the editorial handling by Christian Koeberl and Karsten Piepjohn.

REFERENCES CITED

- Amato, J.M., Aleinikoff, J.N., Akinin, V.V., McClelland, W.C., and Toro, J., 2014, Age, chemistry, and correlations of Neoproterozoic–Devonian igneous rocks of the Arctic Alaska–Chukotka terrane: An overview with new U-Pb ages, in Dumoulin, J.A., and Till, A.B., eds., Reconstruction of a Late Proterozoic and Early Paleozoic Continental Margin—Seward Peninsula and Correlative Rocks of the Arctic Alaska–Chukotka Terrane: Geological Society of America Special Paper 506, p. 29–57, https://doi.org/10.1130/2014.2506(02).
- Amato, J.M., Toro, J., Miller, E.L., Gehrels, G.E., Farmer, G.L., Gottlieb, E.S., and Till, A.B., 2009, Late Proterozoic–Paleozoic evolution of the Arctic Alaska–Chukotka terrane based on U-Pb igneous and detrital zircon ages: Implications for Neoproterozoic paleogeographic reconstructions: Geological Society of America Bulletin, v. 121, p. 1219–1235, https://doi.org/10.1130/B26510.1.
- Anderson, A.V., Wallace, W.K., and Mull, C.G., 1994, Depositional record of a major tectonic transition in northern Alaska: Middle Devonian to Mississippian rift-basin margin deposits, upper Kongakut River region, eastern Brooks Range, Alaska, in Thurston, D.K., and Fujita, K., eds., 1992 Proceedings of the International Conference on Arctic Margins: Anchorage, Alaska, U.S. Department of the Interior, Minerals Management Service, OCS (Outer Continental Shelf) Study MMS 94–0040, p. 71–76.
- Arevalo, R., and McDonough, W.F., 2010, Chemical variations and regional diversity observed in MORB: Chemical Geology, v. 271, p. 70–85, https://doi.org/10.1016/j.chemgeo.2009.12.013.
- Bao, J.S., and Jago, J.B., 2000, Late late Cambrian trilobites from near Birch Inlet, south-western Tasmania: Palaeontology, v. 43, p. 881–917, https:// doi.org/10.1111/1475-4983.00154.
- Béchennec, F., Le Metour, J., Rabu, D., Bourdillon-de-Grissac, C., de Wever, P., Beurrier, M., and Villey, M., 1990, The Hawasina Nappes: Stratigraphy, palaeogeography and structural evolution of a fragment of the south-Tethyan passive continental margin, in Robertson, A.H.F., Searle, M.P., and Ries, A.C., eds., The Geology and Tectonics of the Oman Region: Geological Society, London, Special Publication 49, p. 213–223, https:// doi.org/10.1144/GSL.SP.1992.049.01.14.
- Beranek, L.P., van Staal, C.R., McClelland, W.C., Israel, S., and Mihalynuk, M.G., 2013, Detrital zircon Hf isotopic compositions indicate a northern Caledonian connection for the Alexander terrane: Lithosphere, v. 5, p. 163–168, https://doi.org/10.1130/L255.1.
- Beranek, L.P., Pease, V.L., Hadlari, T., and Dewing, K., 2015, Silurian flysch successions of Ellesmere Island, Arctic Canada, and their significance to northern Caledonian palaeogeography and tectonics: Journal of the Geological Society [London], v. 172, p. 201–212, https://doi.org/10.1144/jgs2014-027.
- Bouvier, A., Vervoort, J.D., and Patchett, P.J., 2008, The Lu-Hf and Sm-Nd isotopic composition of CHUR: Constraints from unequilibrated chondrites and implications for the bulk composition of terrestrial planets: Earth and Planetary Science Letters, v. 273, p. 48–57, https://doi.org/10.1016/j.epsl.2008.06.010.
- Brosgé, W.P., Dutro, J.T., Jr., Mangus, M.D., and Reiser, H.N., 1962, Paleozoic sequences in the eastern Brooks Range, Alaska: American Association of Petroleum Geologists Bulletin, v. 46, p. 2174–2198.
- Cecile, M.P., 2000, Geology of the Northeastern Niddery Lake Map Area, East-Central Yukon and Adjacent Northwest Territories: Geological Survey of Canada Bulletin 553, 120 p., https://doi.org/10.4095/211664.
- Cecile, M.P., Morrow, D.W., and Williams, G.K., 1997, Early Paleozoic (Cambrian to Early Devonian) tectonic framework, Canadian Cordillera: Bulletin of Canadian Petroleum Geology, v. 45, p. 54–74.
- Cecile, M.P., Lane, L.S., Khudoley, A.K., and Kos'ko, M.K., 1999, Lower Paleozoic rocks around today's Arctic Ocean: Two ancestral continents and associated plates; Alaskan rotation unnecessary and unlikely: Polarforschung, v. 69, p. 235–241.

- Chatterton, B.D.E., and Gibb, S., 2016, Furongian (Upper Cambrian) Trilobites from the McKay Group, Bull River Valley, near Cranbrook, Southeastern British Columbia, Canada: Palaeontographica Canadiana 35, 275 p.
- Chew, D.M., and Strachan, R.A., 2014, The Laurentian Caledonides of Scotland and Ireland, in Corfu, F., Gasser, D., and Chew, D.M., eds., New Perspectives on the Caledonides of Scandinavia and Related Areas: Geological Society, London, Special Publication 390, p. 45–91, https://doi.org/10.1144/SP390.16.
- Chien, Y.Y., 1961, Cambrian trilobites from Sandu and Duyan, southern Kweichow: Acta Palaeontologica Sinica, v. 9, p. 91–139.
- Choi, D.K., Lee, J.G., and Sheen, B.C., 2004, Upper Cambrian agnostoid trilobites from the Machari Formation, Yongwol, Korea: Geobios, v. 37, p. 159–189, https://doi.org/10.1016/j.geobios.2003.02.004.
- Colpron, M., and Nelson, J.L., 2011, A Palaeozoic NW Passage and the Timanian, Caledonian and Uralian connections of some exotic terranes in the North American Cordillera, in Spencer, A.M., Embry, A.F., Gautier, D.L., Stoupakova, A.V., and Sørensen, K., eds., Arctic Petroleum Geology: Geological Society, London, Memoir 35, p. 463–484, https://doi.org/10.1144/M35.31.
- Corfu, F., Andersen, T.B., and Gasser, D., 2014, The Scandinavian Caledonides: Main features, conceptual advances and critical questions, in Corfu, F., Gasser, D., and Chew, D.M., eds., New Perspectives on the Caledonides of Scandinavia and Related Areas: Geological Society, London, Special Publication 390, p. 9–43, https://doi.org/10.1144/SP390.25.
- Cox, G.M., Strauss, J.V., Halverson, G.P., Schmitz, M.D., McClelland, W.C., Stevenson, R.S., and MacDonald, F.A., 2015, Kikiktat volcanics of Arctic Alaska—Melting of harzburgitic mantle associated with the Franklin large igneous province: Lithosphere, v. 7, p. 275–295, https://doi.org/10.1130/L435.1.
- Dumoulin, J.A., Harris, A.G., Gagiev, M., Bradley, D.C., and Repetski, J.E., 2002, Lithostratigraphic, conodont, and other faunal links between Lower Paleozoic strata in northern and central Alaska and northeastern Russia, in Miller, E.L., Grantz, A., and Klemperer, S.L., eds., Tectonic Evolution of the Bering Shelf–Chukchi Sea–Arctic Margin and Adjacent Landmasses: Geological Society of America Special Paper 360, p. 291–312, https://doi.org/10.1130/0-8137-2360-4.291.
- Dutro, J.T., Jr., Brosgé, W.P., and Reiser, H.N., 1972, Significance of recently discovered Cambrian fossils and reinterpretation of Neruokpuk Formation, northeastern Alaska: American Association of Petroleum Geologists Bulletin, v. 56, p. 808–815.
- Elliott, T., 2003, Tracers of the slab, in Eiler, J., ed., Inside the Subduction Factory: American Geophysical Union Geophysical Monograph 138, p. 23–45, https://doi.org/10.1029/138GM03.
- Fitton, J.G., 1987, The Cameroon line, West Africa: A comparison between oceanic and continental alkaline volcanism, in Fitton, J.G., and Upton, B.G.J., eds., Alkaline Igneous Rocks: Geological Society, London, Special Publication 30, p. 273–291, https://doi.org/10.1144/GSL.SP.1987.030.01.13.
- Fortey, R.A., 1980, The Ordovician Trilobites of Spitsbergen III, Remaining Trilobites of the Valhallfonna Formation: Norsk Polarinstitutt Skrifter 171, 163 p.
- Gehrels, G.E., and Pecha, M., 2014, Detrital zircon U-Pb geochronology and Hf isotope geochemistry of Paleozoic and Triassic passive margin strata of western North America: Geosphere, v. 10, p. 49–65, https://doi.org/10.1130/GES00889.1.
- Gehrels, G.E., Valencia, V.A., and Ruiz, J., 2008, Enhanced precision, accuracy, efficiency, and spatial resolution of U-Pb ages by laser ablation—multicollector—inductively coupled plasma—mass spectrometry: Geochemistry Geophysics Geosystems, v. 9, Q03017, https://doi.org/10.1029/2007GC001805.
- Goodfellow, W.D., Cecile, M.P., and Leybourne, M.I., 1995, Geochemistry, petrogenesis, and tectonic setting of Lower Paleozoic alkalic and potassic volcanic rocks, northern Canadian Cordilleran miogeocline: Canadian Journal of Earth Sciences, v. 32, no. 8, p. 1236–1254, https://doi.org/10.1139/e95-101.
- Gradstein, F.M., Ogg, J.G., Smith, A.G., and Ogg, G., 2012, The Geologic Time Scale: Cambridge, UK, Cambridge University Press, 1176 p.
- Grant, R.E., 1965, Faunas and Stratigraphy of the Snowy Range Formation (Upper Cambrian) in Southwestern Montana and Northwestern Wyoming: Geological Society of America Memoir 96, 171 p., https://doi .org/10.1130/MEM96-p1.
- Green, D.H., and Ringwood, A.E., 1967, The genesis of basaltic magmas: Contributions to Mineralogy and Petrology, v. 15, p. 103–190, https://doi.org/10.1007/BF00372052.

- Hart, C.J.R., 1986, The Geology of the Old Cabin Creek Massif, Selwyn Basin, Yukon Territory [B.S. thesis]: Hamilton, Ontario, Canada, McMaster University, 111 p.
- Henderson, R.A., 1976, Upper Cambrian (Idamean) trilobites from western Queensland, Australia: Palaeontology, v. 19, p. 325–364.
- Hofmann, A.W., 2003, Sampling mantle heterogeneity through oceanic basalts: Isotopes and trace elements, in Carlson, R.W., ed., Treatise on Geochemistry, Volume 2: The Mantle and Core: Oxford, Elsevier, p. 61–101.
- Hoiland, C.W., Miller, E.L., Pease, V., and Hourigan, J.K., 2017, Detrital zircon U-Pb geochronology and Hf isotope geochemistry of metasedimentary strata in the southern Brooks Range: Constraints on Neoproterozoic– Cretaceous evolution of Arctic Alaska, in Pease, V.L., and Coakley, B.J., eds., Circum-Arctic Lithosphere Evolution: Geological Society, London, Special Publication 460, p. 121–158, https://doi.org/10.1144/SP460.16
- Hooper, P.R., and Hawkesworth, C.J., 1993, Isotopic and geochemical constraints on the origin and evolution of the Columbia River Basalt: Journal of Petrology, v. 34, p. 1203–1246, https://doi.org/10.1093/petrology/34.6.1203.
- Jackson, D.E., 1964, Observations on the sequence and correlation of Lower and Middle Ordovician graptolite faunas of North America: Geological Society of America Bulletin, v. 75, p. 523–534, https://doi.org/10.1130/0016 -7606(1964)75[523:OOTSAC]2.0.CO;2.
- Jaques, A.L., and Green, D.H., 1980, Anhydrous melting of peridotite at 0–15 Kb pressure and the genesis of tholeitic basalts: Contributions to Mineralogy and Petrology, v. 73, p. 287–310, https://doi.org/10.1007/ BF00381447.
- Johnson, B.G., Strauss, J.V., Toro, J., Benowitz, J.A., Ward, W.P., and Hourigan, J.K., 2016, Detrital geochronology of pre-Mississippian strata in the northeastern Brooks Range, Alaska: Insights into the tectonic evolution of northern Laurentia: Lithosphere, v. 8, p. 649–667, https://doi.org/10.1130/L533.1.
- Jones, D.L., Silberling, N.J., Coney, P.J., and Plafker, G., 1987, Lithotectonic Terrane Map of Alaska: U.S. Geological Survey Miscellaneous Field Studies Map MF-874, scale 1:2,500,000.
- Kampunzu, A.B., and Mohr, P., 1991, Magmatic evolution and petrogenesis in the East African Rift System, *in* Kampunzu, A.B., and Lubala, R.T., eds., Magmatism in Extensional Structural Settings: Berlin, Springer, p. 85–136.
- Kelley, J.S., Wrucke, C.T., and Lane, L.S., 1994, Pre-Mississippian rocks in the Clarence and Malcolm Rivers area, Alaska and Yukon Territory, in 1992 Proceedings of the International Conference on Arctic Margins: Anchorage, Alaska, U.S. Department of the Interior, Minerals Management Service, OCS (Outer Continental Shelf) Study MMS 94–0040, p. 59–64.
- Kushiro, I., 2001, Partial melting experiments on peridotite and origin of midocean ridge basalt: Annual Review of Earth and Planetary Sciences, v. 29, p. 71–107, https://doi.org/10.1146/annurev.earth.29.1.71.
- Lane, L.S., 1991, The pre-Mississippian "Neruokpuk Formation," northeastern Alaska and northwestern Yukon: Review and new regional correlation: Canadian Journal of Earth Sciences, v. 28, p. 1521–1533, https://doi .org/10.1139/e91-136.
- Lane, L.S., 2007, Devonian–Carboniferous paleogeography and orogenesis, northern Yukon and adjacent Arctic Alaska: Canadian Journal of Earth Sciences, v. 44, p. 679–694, https://doi.org/10.1139/e06-131.
- Lane, L.S., Kelley, J.S., and Wrucke, C.T., 1995, Stratigraphy and Structure of the Clarence River Area, Yukon–Alaska North Slope: A USGS-GSC Co-Operative Project: Current Research Part E: Geological Survey of Canada Paper 1995-E, p. 1–9, https://doi.org/10.4095/205183.
- Lane, L.S., Gehrels, G.E., and Layer, P.W., 2016, Provenance and paleogeography of the Neruokpuk Formation, northwest Laurentia: An integrated synthesis: Geological Society of America Bulletin, v. 128, p. 239–257, https://doi.org/10.1130/B31234.1.
- Lawver, L.A., Grantz, A., and Gahan, L.M., 2002, Plate kinematic evolution of the present Arctic region since the Ordovician, in Miller, E.L., Grantz, A., and Klemperer, S.L., eds., Tectonic Evolution of the Bering Shelf–Chukchi Sea– Arctic Margin and Adjacent Landmasses: Geological Society of America Special Paper 360, p. 333–358, https://doi.org/10.1130/0-8137-2360-4.333.
- Lazarenko, N.P., Gogin, I.Y., Pegel, T.V., Sukhov, S.S., Abaimova, G.P., Egorova, L.I., Federov, A.B., Raevskaya, E.G., and Ushatinskaya, G.T., 2006, Cambrian stratigraphy of the northeastern Siberian Platform and potential stratotypes of lower boundaries of the proposed Upper Cambrian Chekurovkian and Nelegerian stages in the Ogon'or Formation section at the Khos-Nelege River, *in* Rozanov, A.Y., and Varlamov, A.I., eds., The Cambrian System of the Siberian Platform, Part 2: North-east of

- the Siberian Platform, XIII International Field Conference of the Yakutia, Russia, Cambrian Stage Subdivision Working Group: International Commission on Cambrian Stratigraphy, p. 61–139.
- Leffingwell, E. de K., 1919, The Canning River Region, Northern Alaska: U.S. Geological Survey Professional Paper 109, 251 p.
- Longacre, S.A., 1970, Trilobites of the Upper Cambrian Ptychaspid Biomere, Wilberns Formation, Central Texas: Paleontological Society Memoir 4, 70 p.
- Lu, Y.H., 1956, An Upper Cambrian trilobite faunule from eastern Kweichou: Acta Palaeontologica Sinica, v. 4, p. 365–380.
- Lu, Y.K., and Zhu, Z.L., 1980, Cambrian trilobites from Chuxian-Quanjiao region, Anhui: Memoirs of the Nanjing Institute of Geology and Palaeontology, v. 16, p. 1–33.
- Ludvigsen, R., and Westrop, S.R., 1983, Franconian Trilobites of New York State: New York State Museum Memoir 23, 83 p.
- Ludvigsen, R., Westrop, S.R., and Kindle, C., 1989, Sunwaptan (Upper Cambrian) Trilobites of the Cow Head Group, Western Newfoundland, Canada: Palaeontographica Canadiana 6, 175 p.
- Ludwig, K.R., 2012, User's Manual for Isoplot/Ex, Version 3.75: A Geochronological Toolkit for Microsoft Excel: Berkeley Geochronology Center Special Publication 5, 75 p.
- MacNaughton, R.B., Moynihan, D.P., Roots, C.F., and Crowley, J.L., 2016, New occurrences of *Oldhamia* in eastern Yukon, Canada: Stratigraphic context and implications for Cambrian deep-marine biostratigraphy: Ichnos, v. 23, p. 33–52, https://doi.org/10.1080/10420940.2015.1127232.
- MacPherson, G.J., Phipps, S.P., and Grossman, J.N., 1990, Diverse sources for igneous blocks in Franciscan mélanges, California Coast Ranges: The Journal of Geology, v. 98, p. 845–862, https://doi.org/10.1086/629457.
- McClelland, W.C., Colpron, M., Piepjohn, K., von Gosen, W., Ward, W.P., and Strauss, J.V., 2015, Preliminary detrital zircon geochronology of the Neruokpuk Formation in the Barn Mountains, Yukon, in MacFarlane, K.E., Nordling, M.G., and Sack, P.J., eds., Yukon Exploration and Geology 2014: Whitehorse, Yukon Geological Survey, p. 123–143.
- McDonough, W.F., and Sun, S.-s., 1995, The composition of the Earth: Chemical Geology, v. 120, p. 223–253, https://doi.org/10.1016/0009 -2541(94)00140-4.
- Miller, E.L., Kuznetsov, N., Soboleva, A., Udoratina, O., Grove, M.J., and Gehrels, G.E., 2011, Baltica in the Cordillera?: Geology, v. 39, p. 791–794, https://doi.org/10.1130/G31910.1.
- Miller, E.L., Toro, J., Gehrels, G.E., Amato, J.M., Prokopiev, A., Tuchkova, M.I., Akinin, V.V., Dumitru, T.A., Moore, T.E., and Cecile, M.P., 2006, New insights into Arctic paleogeography and tectonics from U-Pb detrital zircon geochronology: Tectonics, v. 25, TC3013, https://doi.org/10.1029/2005TC001830.
- Moore, T.E., 1987, Geochemistry and the tectonic setting of volcanic rocks of the Franklinian assemblage, central and eastern Brooks Range, in Tailleur, I., and Weimer, P., eds., Alaskan North Slope Geology: Pacific Section, Society of Economic Paleontologists and Mineralogists (SEPM) Publication 50, p. 691–710.
- Moore, T.E., and Churkin, M., Jr., 1984, Ordovician and Silurian graptolite discoveries from the Neruokpuk Formation (sensu lato), northeastern and central Brooks Range, Alaska, *in* Blodgett, R.B., ed., Paleozoic Geology of Alaska and Northwestern Canada Newsletter 1: Anchorage, Alaska Geological Society, p. 21–23.
- Moore, T.E., Wallace, W.K., Bird, K.J., Karl, S.M., Mull, C.G., and Dillon, J.T., 1994, Geology of northern Alaska, in Plafker, G., and Berg, H.C., eds., The Geology of Alaska: Boulder, Colorado, Geological Society of America, The Geology of North America, v. G-1, p. 49–140.
- Mull, C.G., and Anderson, A.V., 1991, Franklinian Lithotectonic Domains, Northeastern Brooks Range, Alaska: Alaska Division of Geological & Geophysical Surveys Public Data File 91–5, 40 p., https://doi.org/10.14509/1472.
- Nelson, L.L., Strauss, J.V., Crockford, P.W., Cox, G.M., Johnson, B.G., Ward, W., Colpron, M., McClelland, W.C., and Macdonald, F.A., 2018, this volume, Geochemical constraints on the provenance of pre-Mississippian sedimentary rocks in the North Slope subterrane of Yukon and Alaska, in Piepjohn, K., Strauss, J.V., Reinhart, L., and McClelland, W.C., eds., Circum-Arctic Structural Events: Tectonic Evolution of the Arctic Margins and Trans-Arctic Links with Adjacent Orogens: Geological Society of American Special Paper 541, Chapter 24, https://doi.org/10.1130/2018.2541(24).
- Palmer, A.R., 1965, Trilobites of the Cambrian Pterocephaliid Biomere in the Great Basin, United States: U.S. Geological Survey Professional Paper 493, 105 p.

- Palmer, A.R., 1968, Cambrian Trilobites of East-Central Alaska, United States: U.S. Geological Survey Professional Paper 559B, 115 p.
- Palmer, A.R., and Halley, R.R., 1979, Physical Stratigraphy and Trilobite Biostratigraphy of the Carrara Formation (Lower and Middle Cambrian) in the Southern Great Basin: U.S. Geological Survey Professional Paper 1047, 131 p.
- Patrick, B.E., and McClelland, W.C., 1995, Late Proterozoic granitic magmatism on Seward Peninsula and a Barentian origin for Arctic Alaska–Chukotka: Geology, v. 23, p. 81–84, https://doi.org/10.1130/0091-7613(1995)023<0081:LPGMOS>2.3.CO;2.
- Pearce, J.A., 1996, A User's Guide to Basalt Discrimination Diagrams: Geological Association of Canada Short Course Notes 12, p. 79–113.
- Pease, V.L., 2011, Eurasian orogens and Arctic tectonics: An overview, in Spencer, A.M., Embry, A.F., Gautier, D.L., Stoupakova, A.V., and Sørensen, K., eds., Arctic Petroleum Geology: Geological Society, London, Memoir 35, p. 311–324.
- Pegel, T.V., 2000, Evolution of trilobite biofacies in Cambrian basins of the Siberian Platform: Journal of Paleontology, v. 74, p. 1000–1019, https:// doi.org/10.1017/S0022336000017571.
- Peng, S., 1992, Upper Cambrian Biostratigraphy and Trilobite Faunas of the Cili-Taoyuan Area, Northwestern Hunan, China: Association of Australasian Palaeontologists Memoir 13, 119 p.
- Peng, S., and Robison, R.A., 2000, Agnostid Biostratigraphy across the Middle–Upper Cambrian Boundary in Hunan, China: Paleontological Society Memoir 53, 104 p.
- Pillevuit, A., Marcoux, J., Stampfli, G., and Baud, A., 1997, The Oman Exotics: A key to the understanding of the Neotethyan geodynamic evolution: Geodinamica Acta, v. 10, p. 209–238, https://doi.org/10.1080/09853111 .1997.11105303.
- Pratt, B.R., 1992, Trilobites of the Marjuman and Steptoean Stages (Upper Cambrian), Rabbitkettle Formation, Southern Mackenzie Mountains, Northwest Canada: Palaeontographica Canadiana 9, 179 p.
- Pyle, L., and Barnes, C., 2003, Lower Paleozoic stratigraphic and biostratigraphic correlations in the Canadian Cordillera: Implications for the tectonic evolution of the Laurentian margin: Canadian Journal of Earth Sciences, v. 40, p. 1739–1753, https://doi.org/10.1139/e03-049.
- Rasetti, F., 1944, Upper Cambrian trilobites from the Levis Conglomerate: Journal of Paleontology, v. 18, p. 229–258.
- Raymond, P.E., 1924, New Upper Cambrian and Lower Ordovician trilobites from Vermont: Proceedings of the Boston Society of Natural History, v. 37, p. 389–446.
- Reiser, H.N., 1970, Northeastern Brooks Range—A surface expression of the Prudhoe Bay section, in Adkison, W.L., and Brosgé, W.P., eds., Proceedings of the Geological Seminar on the North Slope of Alaska: Los Angeles, California, Pacific Section, American Association of Petroleum Geologists, p. K1–K13.
- Reiser, H.N., Brosge, W.P., Dutro, J.T., Jr., and Detterman, R.L., 1980, Geologic Map of the Demarcation Point Quadrangle, Alaska: U.S. Geological Survey Miscellaneous Investigations Series Map 1133, scale 1:250,000.
- Robinson, J.A.C., and Wood, B.J., 1998, The depth of the spinel to garnet transition at the peridotite solidus: Earth and Planetary Science Letters, v. 164, p. 277–284, https://doi.org/10.1016/S0012-821X(98)00213-1.
- Salters, V.J.M., and Stracke, A., 2004, Composition of the depleted mantle: Geochemistry Geophysics Geosystems, v. 5, Q05B07, https://doi.org/ 10.1029/2003GC000597.
- Searle, M.P., and Graham, G.M., 1982, "Oman Exotics"—Oceanic carbonate build-ups associated with the early stages of continental rifting: Geology, v. 10, p. 43–49, https://doi.org/10.1130/0091-7613(1982)10<43:OECBAW>2.0.CO;2.
- Shergold, J.H., 1977, Classification of the trilobite *Pseudagnostus*: Palaeontology, v. 20, p. 69–100.
- Shergold, J.H., 1980, Late Cambrian Trilobites from the Chatsworth Limestone, Western Queensland: Australian Bureau of Mineral Resources, Geology and Geophysics Bulletin 186, 111 p.
- Shergold, J.H., Laurie, J.R., and Sun, X., 1990, Classification and Review of the Trilobite Order Agnostida Salter, 1864: An Australian Perspective: Australian Bureau of Mineral Resources, Geology and Geophysics Report 296, 93 p.
- Shervais, J.W., 1982, Ti-V plots and the petrogenesis of modern and ophiolitic lavas: Earth and Planetary Science Letters, v. 59, p. 101–118, https://doi.org/10.1016/0012-821X(82)90120-0.
- Shervais, J.W., and Kimbrough, D.L.K., 1987, Alkaline and transitional subalkaline metabasalts in the Franciscan Complex mélange, California, *in*

- Morris, E.M., and Pasteris, J.D., eds., Mantle Metasomatism and Alkaline Magmatism: Geological Society of America Special Paper 215, p. 165–182, https://doi.org/10.1130/SPE215-p165.
- Stitt, J.H., 1971, Late Cambrian and Earliest Ordovician Trilobites, Timbered Hills and Lower Arbuckle Groups, Western Arbuckle Mountains, Murray County, Oklahoma: Oklahoma Geological Survey Bulletin 110, 83 p.
- Strauss, J.V., Macdonald, F.A., Taylor, J.F., Repetski, J.E., and McClelland, W.C., 2013, Laurentian origin for the North Slope of Alaska: Implications for the tectonic evolution of the Arctic: Lithosphere, v. 5, p. 477–482, https://doi.org/10.1130/L284.1.
- Strauss, J.V., Hoiland, C.W., Ward, W.P., Johnson, B.G., Nelson, L.L., and McClelland, W.C., 2017, Orogen transplant: Taconic-Caledonian arc magmatism in the central Brooks Range of Alaska: Geological Society of America Bulletin, v. 129, p. 649–676, https://doi.org/10.1130/B31593.1.
- Strauss, J.V., Johnson, B.G., Colpron, M., Nelson, L.L., Perez, J.L., Benowitz, J.A., Ward, W.P., and McClelland, W.C., 2018, this volume, Pre-Mississippian stratigraphy and provenance of the North Slope subterrane of Arctic Alaska II: Basinal rocks of the northeastern Brooks Range and their significance in circum-Arctic evolution, in Piepjohn, K., Strauss, J.V., Reinhardt, L., and McClelland, W.C., eds., Circum-Arctic Structural Events: Tectonic Evolution of the Arctic Margins and Trans-Arctic Links with Adjacent Orogens: Geological Society of America Special Paper 541, Chapter 23, https://doi.org/10.1130/2018.2541(23).
- Sun, S.-s., and McDonough, W.F., 1989, Chemical and isotopic systematics of oceanic basalts: Implications for mantle composition and processes, in Saunders, A.D., and Norry, M.J., eds., Magmatism in the Ocean Basins: Geological Society, London, Special Publication 42, p. 313–345, https:// doi.org/10.1144/GSL.SP.1989.042.01.19.
- Sweeney, J.F., 1982, Mid-Palaeozoic travels of Arctic-Alaska: Nature, v. 298, p. 647–649, https://doi.org/10.1038/298647a0.
- Tarduno, J.A., McWilliams, M., Debiche, M.G., Sliter, W.V., and Blake, M.C., 1985, Franciscan Complex Calera limestones: Accreted remnants of Farallon plate oceanic plateaus: Nature, v. 317, p. 345–347, https://doi.org/10.1038/317345a0.
- Taylor, J.F., Brezinski, D.K., Repetski, J.E., and Welsh, N.M., 2009, The Adamstown submergence event: Faunal and sedimentological record of a late Cambrian (Furongian) transgression in the Appalachian region, in Laurie, J.R., ed., Cambro-Ordovician Studies IV: Association of Australasian Palaeontologists Memoir 37, p. 641–666.
- Taylor, J.F., Repetski, J.E., Loch, J.D., and Leslie, S.A., 2012, Biostratigraphy and chronostratigraphy of the Cambrian–Ordovician Great American Carbonate Bank, in Derby, J.R., Fritz, R.D., Longacre, S.A., Morgan, W.A., and Sternbach, C.A., eds., The Great American Carbonate Bank: The Geology and Economic Resources of the Cambrian–Ordovician Sauk Megasequence of Laurentia: American Association of Petroleum Geologists Memoir 98, p. 15–35.
- van Staal, C.R., and Barr, S.M., 2012, Lithospheric architecture and tectonic evolution of the Canadian Appalachians and associated Atlantic margin, in Percival, J.A., Cook, F.A., and Clowes, R.M., eds., Tectonic Styles in Canada: The LITHOPROBE Perspective: Geological Association of Canada Special Paper 49, p. 41–45.
- van Staal, C.R., Dewey, J.F., Niocaill, C.M., and McKerrow, W.S., 1998, The Cambrian–Silurian tectonic evolution of the Northern Appalachians and British Caledonides: History of a complex, west and southwest Pacifictype segment of Iapetus: Geological Society, London, Special Publication 143, p. 197–242, https://doi.org/10.1144/GSL.SP.1998.143.01.17.
- Varlamov, A.I., Pak, K.L., and Rosova, A.V., 2006, The Upper Cambrian of the Chopko River section, Norilsk region, northwestern Siberian Platform: Stratigraphy and trilobites: Palaeontological Journal, v. 40, Supplement 1, p. S1–S56.
- Vervoort, J.D., and Blichert-Toft, J., 1999, Evolution of the depleted mantle: Hf isotope evidence from juvenile rocks through time: Geochimica et Cosmochimica Acta, v. 63, p. 533–556, https://doi.org/10.1016/S0016 -7037(98)00274-9.
- Vervoort, J.D., and Patchett, P.J., 1996, Behavior of hafnium and neodymium isotopes in the crust: Constraints from Precambrian crustally derived granites: Geochimica et Cosmochimica Acta, v. 60, p. 3717–3733, https:// doi.org/10.1016/0016-7037(96)00201-3.
- Vervoort, J.D., Patchett, P.J., Blichert-Toft, J., and Albarède, F., 1999, Relation-ships between Lu-Hf and Sm-Nd isotopic systems in the global sedimentary system: Earth and Planetary Science Letters, v. 168, p. 79–99, https://doi.org/10.1016/S0012-821X(99)00047-3.

- Wallace, W.K., and Hanks, C.L., 1990, Structural provinces of the northeastern Brooks Range, Arctic National Wildlife Refuge, Alaska: American Association of Petroleum Geologists Bulletin, v. 74, p. 1100–1118.
- Wendt, I., and Carl, C., 1991, The statistical distribution of the mean squared weighted deviation: Chemical Geology–Isotope Geoscience Section, v. 86, p. 275–285, https://doi.org/10.1016/0168-9622(91)90010-T.
- Westrop, S.R., 1986, Trilobites of the Upper Cambrian Sunwaptan Stage, Southern Canadian Rocky Mountains, Alberta: Palaeontographica Canadiana 3, 179 p.
- Westrop, S.R., 1995, Sunwaptan and Ibexian (Upper Cambrian–Lower Ordovician) Trilobites of the Rabbitkettle Formation, Mountain River Region, Northern Mackenzie Mountains, Northwest Canada: Palaeontographica Canadiana 12, 75 p.
- Westrop, S.R., and Eoff, J.D., 2012, Late Cambrian (Furongian: Paibian, Steptoean) agnostoid arthropods from the Cow Head Group, western Newfoundland: BioOne, v. 86, p. 201–237, https://doi.org/10.1666/11-034.1.
- Westrop, S.R., Eoff, J.D., Ng, T.-W., Dengler, A.A., and Adrain, J.M., 2008, Classification of the late Cambrian (Steptoean) trilobite genera *Cheilo-*

- cephalus Berkey, 1898 and Oligometopus Resser, 1936 from Laurentia: Canadian Journal of Earth Sciences, v. 45, p. 725–744, https://doi.org/10.1139/E08-026.
- Wilson, J.L., 1951, Franconian trilobites of the central Appalachians: Journal of Paleontology, v. 25, p. 617–654.
- Winchester, J.A., and Floyd, P.A., 1977, Geochemical discrimination of different magma series and their differentiation products using immobile elements: Chemical Geology, v. 20, p. 325–343, https://doi.org/10.1016/0009-2541(77)90057-2.
- Yoder, H.S., and Tilley, C.E., 1962, Origin of basalt magmas: An experimental study of natural and synthetic rock systems: Journal of Petrology, v. 3, p. 342–532, https://doi.org/10.1093/petrology/3.3.342.

Manuscript Accepted by the Society 8 May 2018